AMERICAN SOCIETY FOR MICROBIOLOGY | Applied and Environmental Microbiology®

GENETICS AND MOLECULAR BIOLOGY

Regulator LdhR and D-Lactate Dehydrogenase LdhA of *Burkholderia multivorans* Play Roles in Carbon Overflow and in Planktonic Cellular Aggregate Formation

Inês N. Silva,[a] Marcelo J. Ramires,[a] Lisa A. Azevedo,[a] Ana R. Guerreiro,[a] Andreia C. Tavares,[a]* Jörg D. Becker,[b] Leonilde M. Moreira[a,c]

IBB, Institute for Bioengineering and Biosciences, Instituto Superior Técnico (IST), Lisbon, Portugal[a]; Instituto Gulbenkian de Ciência, Oeiras, Portugal[b]; Department of Bioengineering, IST, Universidade de Lisboa, Lisbon, Portugal[c]

ABSTRACT LysR-type transcriptional regulators (LTTRs) are the most commonly found regulators in *Burkholderia cepacia* complex, comprising opportunistic pathogens causing chronic respiratory infections in cystic fibrosis (CF) patients. Despite LTTRs being global regulators of pathogenicity in several types of bacteria, few have been characterized in *Burkholderia*. Here, we show that gene *ldhR* of *B. multivorans* encoding an LTTR is cotranscribed with *ldhA* encoding a D-lactate dehydrogenase and evaluate their implication in virulence traits such as exopolysaccharide (EPS) synthesis and biofilm formation. A comparison of the wild type (WT) and its isogenic Δ*ldhR* mutant grown in medium with 2% D-glucose revealed a negative impact on EPS biosynthesis and on cell viability in the presence of LdhR. The loss of viability in WT cells was caused by intracellular acidification as a consequence of the cumulative secretion of organic acids, including D-lactate, which was absent from the Δ*ldhR* mutant supernatant. Furthermore, LdhR is implicated in the formation of planktonic cellular aggregates. WT cell aggregates reached 1,000 μm in size after 24 h in liquid cultures, in contrast to Δ*ldhR* mutant aggregates that never grew more than 60 μm. The overexpression of D-lactate dehydrogenase LdhA in the Δ*ldhR* mutant partially restored the formed aggregate size, suggesting a role for fermentation inside aggregates. Similar results were obtained for surface-attached biofilms, with WT cells producing more biofilm. A systematic evaluation of planktonic aggregates in *Burkholderia* CF clinical isolates showed aggregates in 40 of 74. As CF patients' lung environments are microaerophilic and bacteria are found as free aggregates/biofilms, LdhR and LdhA might have central roles in adapting to this environment.

IMPORTANCE Cystic fibrosis patients often suffer from chronic respiratory infections caused by several types of microorganisms. Among them are the *Burkholderia cepacia* complex bacteria, which cause progressive deterioration of lung function that, in some patients, might develop into fatal necrotizing pneumoniae with bacteremia, known as "cepacia syndrome." *Burkholderia* pathogenesis is multifactorial as they express several virulence factors, form biofilms, and are highly resistant to antimicrobial compounds, making their eradication from the CF patients' airways very difficult. As *Burkholderia* is commonly found in CF lungs in the form of cell aggregates and biofilms, the need to investigate the mechanisms of cellular aggregation is obvious. In this study, we demonstrate the importance of a D-lactate dehydrogenase and a regulator in regulating carbon overflow, cellular aggregates, and surface-attached biofilm formation. This not only enhances our understanding of *Burkholderia* patho-

Received 17 June 2017 **Accepted** 17 July 2017

Accepted manuscript posted online 21 July 2017

Citation Silva IN, Ramires MJ, Azevedo LA, Guerreiro AR, Tavares AC, Becker JD, Moreira LM. 2017. Regulator LdhR and D-lactate dehydrogenase LdhA of *Burkholderia multivorans* play roles in carbon overflow and in planktonic cellular aggregate formation. Appl Environ Microbiol 83:e01343-17. https://doi.org/10.1128/AEM.01343-17.

Editor Ning-Yi Zhou, Shanghai Jiao Tong University

Address correspondence to Leonilde M. Moreira, lmoreira@tecnico.ulisboa.pt.

* Present address: Andreia C. Tavares, Instituto de Tecnologia Química e Biológica António Xavier, ITQB NOVA, Oeiras, Portugal.

genesis but can also lead to the development of drugs against these proteins to circumvent biofilm formation.

KEYWORDS LysR family transcriptional regulator, D-lactate dehydrogenase, *Burkholderia multivorans*, planktonic cellular aggregates, biofilms, exopolysaccharide, cystic fibrosis

Burkholderia cepacia complex comprises bacteria ubiquitous in the environment but is also responsible for persistent infections in the airways of cystic fibrosis (CF) sufferers, strongly contributing to lung function deterioration (1). *Burkholderia* may grow as a single cell, but it is often found in small clusters such as the ones identified in the airways of CF patients (2). To cope with the different environments, these bacteria are equipped with a wide range of metabolic functions and virulence traits, reflected in their genome size ranging from 6 to 9 Mbp (3, 4). One such trait shared by many *B. cepacia* complex strains is the expression of the mucoid phenotype due to the biosynthesis of exopolysaccharides (EPSs) (5, 6). One of those EPSs, cepacian, has been implicated in biofilm formation, inhibition of neutrophil chemotaxis, protection against phagocytosis by human neutrophils, neutralization of reactive oxygen species *in vitro*, facilitation of persistent bacterial infection in animal models, and protection against abiotic stressors (7–12). The synthesis in large amounts of this polymeric compound requires a high carbon-to-nitrogen ratio, with mannitol or glucose as the commonly used carbon source (6–8). One particular feature of glucose metabolism in *B. cepacia* complex bacteria is the presence of alternative routes for its conversion into gluconate-6-phosphate (6P) prior to entry into the Entner-Doudoroff pathway, the direct oxidative pathway mediated by the activities of membrane-associated glucose and gluconate dehydrogenases, and the phosphorylative pathway mediated by glucokinase and an NADP-dependent glucose-6P dehydrogenase (Fig. 1) (13). The main utilization of one pathway or another is dependent on the glucose source and is strain specific (14). The sugar used as the carbon source for EPS biosynthesis needs to be fed into the central metabolic pathways, and the required activated sugar-nucleotide precursors need to be synthesized. Then, these sugar-nucleotide precursors are assembled into repeating units that are subsequently polymerized, and EPS chains are secreted to the external milieu (5).

Although genes involved in cepacian biosynthesis have already been described (7, 15), the regulation of transcription of those *bce-I* and *bce-II* gene clusters remains mostly unknown. To understand the mechanisms regulating EPS production, Silva and coworkers compared the transcriptomes of mucoid and nonmucoid clonal isolates of *Burkholderia multivorans*, leading to the identification of a putative LysR-type transcriptional regulator (LTTR) whose expression was downregulated in the nonmucoid isolate (16). This LTTR is located upstream of a gene encoding a putative D-lactate dehydrogenase, an enzyme that reversibly converts pyruvate into D-lactate. Besides the important role of D-lactate dehydrogenase in fermentation and energy production under oxygen-limiting conditions, this metabolic conversion has been shown as required for microcolony formation, a hallmark of biofilm architecture in *Pseudomonas aeruginosa* (17), especially in association with CF lung infections (2, 18). Petrova and coworkers, by studying the role of the two-component regulator MifR, demonstrated that inactivation of genes involved in pyruvate utilization or the depletion of pyruvate from the growth medium abrogated microcolony formation, and pyruvate supplementation significantly increased microcolony formation (17). Although that study revealed that MifR-dependent microcolony formation is associated with stressful, oxygen-limiting yet electron-rich conditions, other mechanisms seem also to be implicated in microcolony formation in *P. aeruginosa*. Indeed, the LTTR BvlR of *P. aeruginosa* PA14 was implicated in tight microcolony formation, possibly mediated through the repression of fimbria-based surface attachment (19). Tight microcolonies (also named planktonic cellular aggregates) are a mode of biofilm that does not require a surface to attach to. Instead, cells self-aggregate to form free-floating suspended biofilms. In another study, the

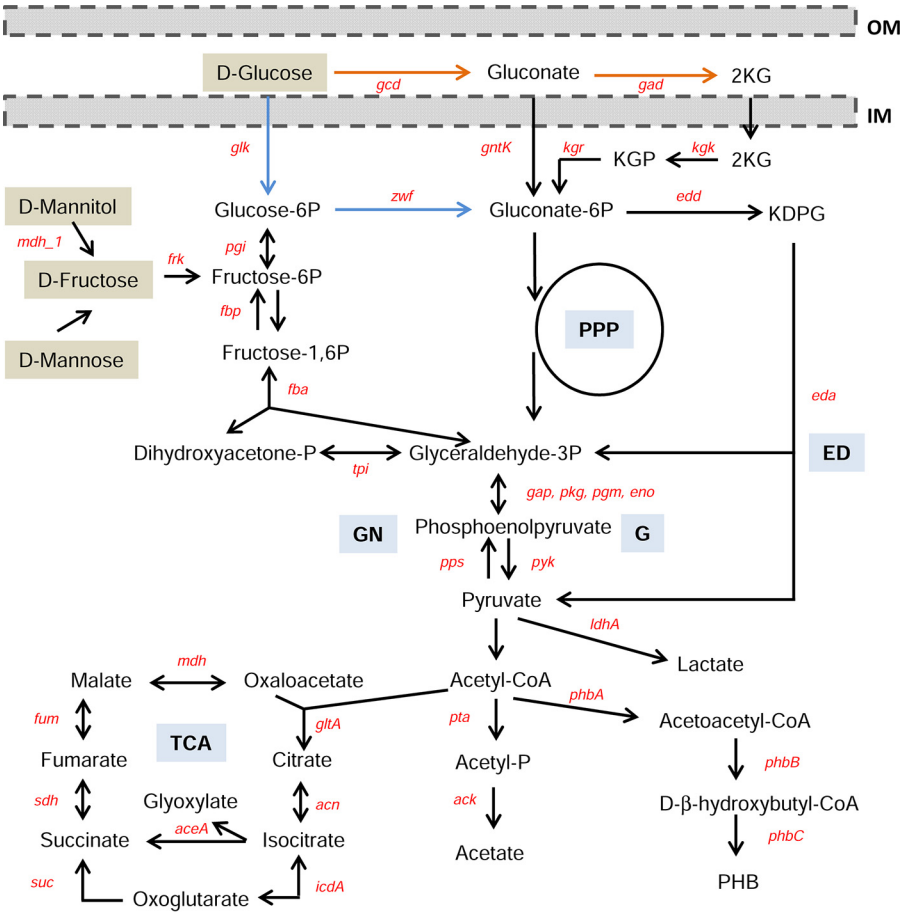

FIG 1 Alternative pathways of gluconate-6P formation by dissimilation of glucose in *Burkholderia*. Glucose utilization can follow the direct oxidative pathway (orange arrows) or the phosphorylative pathway (blue arrows). Catabolism of other monomeric carbon sources (marked with brown boxes) is also indicated. Central metabolic pathways are glycolysis (G), Entner-Doudoroff pathway (ED), pentose-phosphate pathway (PPP), tricarboxylic acid (TCA) cycle, and gluconeogenesis (GN). Other abbreviations: 2KG, 2-ketogluconate; KGP, 2-ketogluconate-6P; KDPG, 2-keto-3-deoxy-gluconate-6P; *gcd*, glucose dehydrogenase; *gad*, gluconate dehydrogenase; *gntK*, gluconokinase; *kgk*, 2-ketogluconokinase; *kgr*, KGP reductase; *zwf*, glucose-6P dehydrogenase; *glk*, glucokinase; *edd*, glucose-6P dehydratase; *eda*, KDPG aldolase; *tpi*, triose isomerase; *fba*, fructose-1,6P aldolase; *fbp*, fructose-1,6P phosphatase; *pgi*, phosphoglucoisomerase; *mdh_1*, mannitol dehydrogenase; *aceA*, isocitrate lyase; *frk*, fructokinase; *ldhA*, D-lactate dehydrogenase; *phbA*, β-ketothiolase; *phbB*, acetoacetyl-coenzyme A reductase; *phbC*, poly-β-hydroxybutyrate synthase; *gltA*, citrate synthase; *acn*, aconitate hydratase; *icdA*, isocitrate dehydrogenase; *suc*, succinate-coenzyme A transferase; *sdh*, succinate dehydrogenase/fumarate reductase; *fum*, fumarate hydratase; *mdh*, malate dehydrogenase; *gap*, glyceraldehyde-3P dehydrogenase; *pkg*, phosphoglycerate kinase; *pgm*, phosphoglycerate mutase; *eno*, phosphopyruvate hydratase; *pta*, phosphate acetyltransferase; *ack*, acetate kinase; *pps*, phosphoenolpyruvate synthase; *pyk*, pyruvate kinase; PHB, poly-β-hydroxybutyrate; IM, inner membrane; and OM, outer membrane. This simplified catabolic pathway was based on reactions available for *B. multivorans* ATCC 17616 from the Kyoto Encyclopedia of Genes and Genomes (KEGG) database.

free-floating cellular aggregates formed by *P. aeruginosa* PAO1 were analyzed by microscopy, with data showing that they comprise up to 90% of the total planktonic biomass, ranging from 10 to 400 μm in diameter and dispersing into single cells upon carbon, nitrogen, or oxygen limitation (20). During growth, these cellular aggregates contain densely packed viable cells but upon starvation, cell death increases and metabolites and bacteriophages are released to the supernatant.

In this work, we asked whether the identified *B. multivorans* ATCC 17616 LTTR (Bmul_2557) plays a role at the interface between metabolism and pathogenesis, namely, by governing carbon overflow, EPS production, and cellular aggregate/biofilm formation. To address these questions, we made use of a *Bmul_2557* mutant and evaluated EPS production with different carbon sources and measured carbon con-

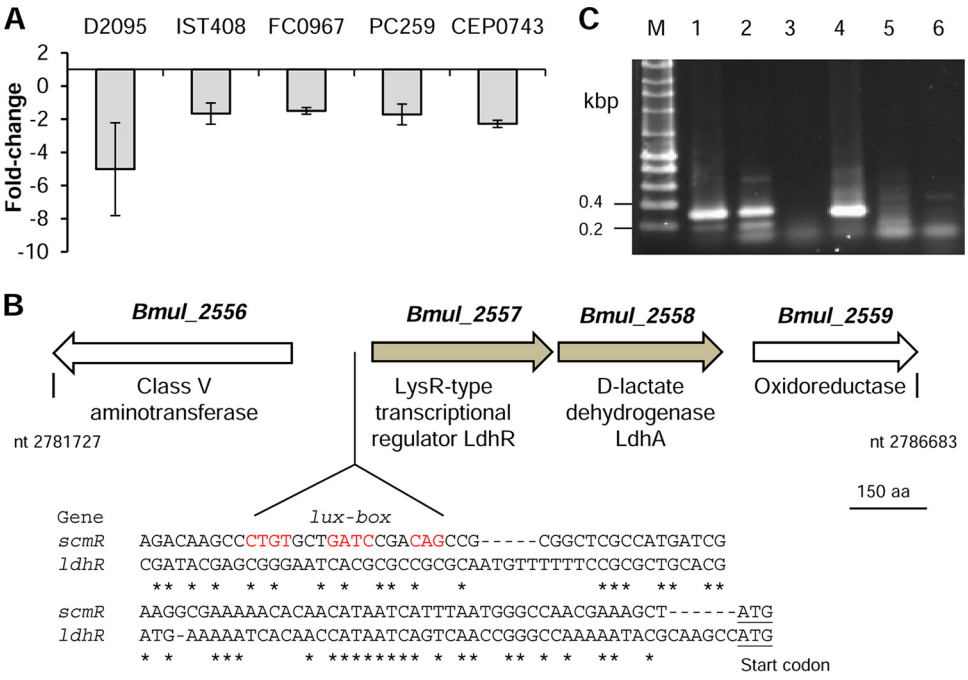

FIG 2 LdhR regulator shows decreased expression in nonmucoid variants derived from mucoid *Burkholderia* strains and is cotranscribed with *ldhA*. (A) Expression by qRT-PCR of *ldhR* in nonmucoid variants compared with those in the respective mucoid parental strains of *B. multivorans* D2095, *B. contaminans* IST408, *B. anthina* FC0967, *B. vietnamiensis* PC259, and *B. dolosa* CEP0743. (B) In *B. multivorans* ATCC 17616, the genomic region containing *ldhR* and the flanking regions is located in chromosome 1 between the nucleotide positions indicated in the figure. The new NCBI locus tags for the indicated genes are *BMUL_RS12975* (*Bmul_2556*), *BMUL_RS12980* (*Bmul_2557*), *BMUL_RS12985* (*Bmul_2558*), and *BMUL_RS12990* (*Bmul_2559*). Nucleotide regions upstream of genes *ldhR* and *scmR* showing a *lux* box sequence (conserved residues in red) preceding the *scmR* gene of *B. thailandensis* E264, which is absent from the *ldhR* upstream region. Asterisks denote conserved nucleotides between the two regions. The putative start codons are underlined. (C) Reverse transcription-PCR showing the cotranscription of *ldhR* and *ldhA* in *B. multivorans* ATCC 17616 grown for 18 h in S medium with 2% D-mannitol. The image shows the amplification from genomic DNA (1), cDNA (2), or total RNA (3) of the 319-bp region comprising the end of *ldhR* and beginning of *ldhA* and amplification from genomic DNA (4), cDNA (5), or total RNA (6) of the 305-bp region comprising the end of *ldhA* and beginning of *Bmul_2559*. M, DNA marker; nt, nucleotides; aa, amino acids.

sumption and metabolic end products, as well as cellular aggregates and biofilm formation. This LTTR, through direct or indirect regulation of the expression of a D-lactate dehydrogenase-encoding gene and possibly other genes, was found to have a significant influence on cellular aggregates and attached biofilm formation but a negative effect on polysaccharide biosynthesis. Furthermore, it regulated the overflow products generated in excess of glucose and similar sugars. Our data support a role for Bmul_2557 LTTR as a key regulator at the boundary between metabolic performance and virulence of *B. multivorans*.

RESULTS

Expression of *Bmul_2557* is decreased in nonmucoid variants. Previous work on the nonmucoid *B. multivorans* D2214 and the clonal mucoid D2095 CF isolates revealed that the gene homolog of *Bmul_2557* from *B. multivorans* ATCC 17616 encoding a putative LTTR had decreased expression in the nonmucoid isolate (16). To assess whether this gene could have a role in the expression of the mucoid phenotype due to cepacian production, its expression level was measured in several stress-induced nonmucoid variants derived from mucoid strains of different *Burkholderia cepacia* complex species (11) grown in S medium with 2% D-mannitol. In agreement with the previous finding in *B. multivorans* D2214/D2095 isolates, the transcription of the *Bmul_2557* gene homologue was decreased in all tested nonmucoid variants relative to that in the respective mucoid parental strain *B. multivorans* D2095, *B. contaminans* IST408, *B. anthina* FC0967, *B. vietnamiensis* PC259, and *B. dolosa* CEP0743 (Fig. 2A).

The *Bmul_2557* gene, tentatively named *ldhR* (lactate dehydrogenase regulator), is located on chromosome 1 of the soil isolate *B. multivorans* ATCC 17616. Located downstream and in the same orientation is the gene *Bmul_2558*, encoding a putative D-lactate dehydrogenase (LdhA) (Fig. 2B). A comparison of the region upstream of *ldhR* with that of the characterized homolog *scmR* from *Burkholderia thailandensis* E264, whose expression is known to be induced by quorum sensing and has a *lux*-box (21), showed the absence of such a conserved region in *B. multivorans* (Fig. 2B). *In silico* analysis predicts an operonic structure for *ldhR* and *ldhA* genes. Reverse transcription-PCR (RT-PCR) experiments on wild-type (WT) cells grown for 18 h in S medium with D-mannitol confirmed their cotranscription and that *Bmul_2559* belongs to another transcriptional unit (Fig. 2C).

LdhR and LdhA display conserved domains of LTTR regulators and D-lactate dehydrogenases, respectively. *In silico* analysis indicated a high conservation of the genomic location of genes *ldhR* and *ldhA* within the *Burkholderia* genus. From the 673 strains whose genome sequences are available at the Burkholderia Genome Database (Mai, 2017), only 9 lack the *ldhR* gene homolog, while 18 do not have the *ldhA* gene homolog. None of these 27 strains are from the *Burkholderia cepacia* complex. A search for homology at the amino acid level between LdhR and other characterized LTTRs indicated that the highest degree of similarity is within the N-terminal helix-turn-helix domain responsible for binding DNA (see Fig. S1A in the supplemental material). The best characterized homolog is ScmR of *Burkholderia thailandensis* E264, showing 65% identity (77% similarity). Some amino acid residues important for DNA binding identified by mutagenesis in proteins CrgA, CysB, and OxyR (22) are also conserved in LdhR from *B. multivorans*. The less conserved C-terminal region, where the coinducer domain is located, has some homology to sugar-binding domains present in ABC transporters and other sugar-binding proteins, suggesting that a sugar-derived metabolite might be involved in LdhR activation.

Protein LdhA is homologous to members of the superfamily of NAD-dependent D-isomer-specific 2-hydroxyacid dehydrogenases. An alignment of the amino acid sequence of LdhA with those of *B. thailandensis* E264 and other D-lactate dehydrogenases, which had their tridimensional structures determined, showed conservation of important residues in both the nucleotide-binding domain and the catalytic domain, as exemplified by the conservation of R^{235} and E^{264}, involved in substrate binding, and D^{259} and H^{296}, involved in catalysis (Fig. S1B).

To substantiate the putative function of LdhA as a D-lactate dehydrogenase, a phylogenetic analysis of the family of D-isomer-specific 2-hydroxyacid dehydrogenases was performed. Based on PROSITE pattern_1, we aligned 185 proteins from the families of D-lactate dehydrogenase (D-LDH), D-3-phosphoglycerate dehydrogenase (SERA), erythronate-4-phosphate dehydrogenase (PDXB), formate dehydrogenase (FDH), glyoxylate/hydroxypyruvate reductase (GHPR), and C-terminal binding protein (CTBP). The phylogenetic analysis shows clustering of the proteins according to substrate specificity, with LdhA from *B. multivorans* ATCC 17616 grouping together with D-lactate dehydrogenases from *Escherichia coli*, *Lactobacillus plantarum*, *Streptococcus agalactiae*, *Staphylococcus aureus*, and *Treponema pallidum* (Fig. 3).

LdhR regulator has a negative effect in EPS production. To test the hypothesis that the LdhR regulator is involved in EPS production, *B. multivorans* ATCC 17616 and the Δ*ldhR* deletion mutant were grown in S medium with different carbon sources for 3 days. In the presence of 2% D-galactose, D-fructose, D-mannitol, or D-mannose, the mutant produced approximately 32 to 45% more EPS than the WT strain (Fig. 4A). In medium supplemented with 2% D-glucose, the WT strain was unable to produce EPS, while the Δ*ldhR* mutant produced approximately 6 g/liter.

To test whether introducing the *ldhR* gene in the mutant would decrease EPS production, a complementation experiment was performed by expressing *ldhR* from pMM137-2. EPS quantification in medium with the different sugars showed that the amount was not significantly different from that of the mutant carrying the empty

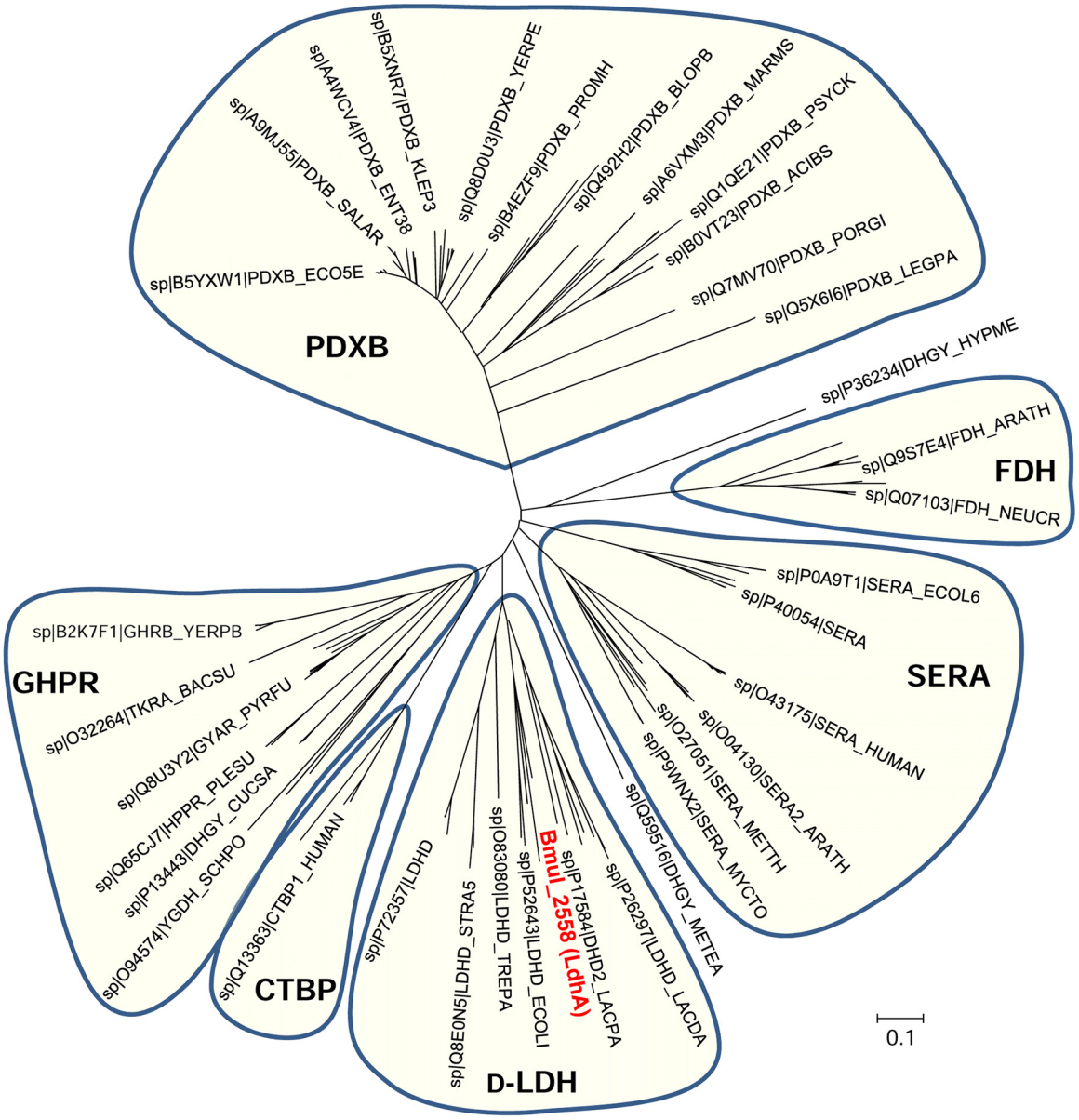

FIG 3 Unrooted neighbor-joining tree of the D-isomer-specific 2-hydroxyacid dehydrogenase superfamily (PROSITE entry PDOC00063_pattern_1). The evolutionary history was inferred using the neighbor-joining method. The analysis involved 185 amino acid sequences. All positions containing gaps and missing data were eliminated. Sequences clustering together and representing separate enzymatic subgroups are shaded. D-LDH, D-lactate dehydrogenases; SERA, D-3-phosphoglycerate dehydrogenases; PDXB, erythronate-4-phosphate dehydrogenases; FDH, formate dehydrogenases; GHPR, glyoxylate/hydroxypyruvate reductases; CTBP, C-terminal binding proteins. *B. multivorans* LdhA is in red font.

vector (data not shown), suggesting a possible polar effect of the trimethoprim resistance cassette replacing *ldhR* on *ldhA* gene expression, as will be demonstrated in the next section. Due to this observation, genes *ldhR* and *ldhA* were expressed simultaneously from their own promoter region cloned into plasmid pARG015-1. When grown in the presence of D-mannose or D-mannitol, there was indeed a reduction in the amount of EPS produced by overexpression of *ldhRA* either in the mutant or in the WT (Fig. 4B). In the presence of D-glucose, the Δ*ldhR* mutant expressing *ldhRA* genes produced no EPS, restoring the phenotype to that of the WT strain. Similarly, the overexpression of both genes in the WT strain confirmed the loss of EPS production (Fig. 4B). The expression of *ldhA* in the Δ*ldhR* mutant had an effect similar to that of expressing both *ldhRA* genes (data not shown). Altogether, these results suggest a negative effect of *ldhR* and *ldhA* gene products on the biosynthesis of EPS.

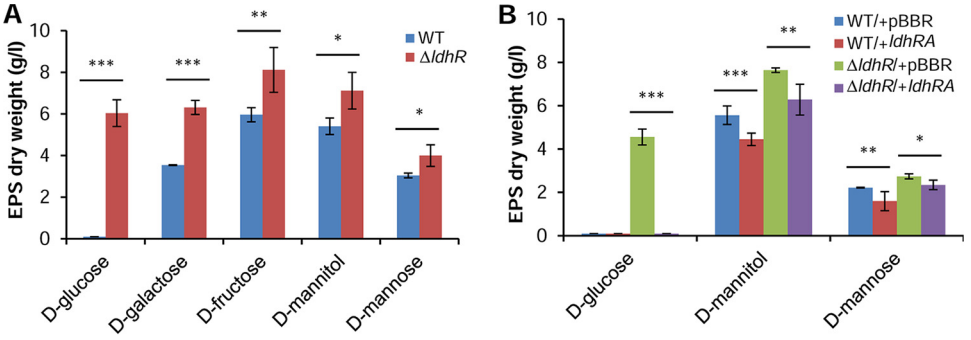

FIG 4 LdhR decreases exopolysaccharide production. (A) Production of EPS by the WT *B. multivorans* ATCC 17616 (WT) and the Δ*ldhR* mutant in the presence of different sugars as the main carbon source for 3 days at 37°C. EPS production is expressed as ethanol precipitate (dry weight) (g/liter). A significantly greater amount of EPS was produced by the Δ*ldhR* mutant. *, $P < 0.05$; **, $P < 0.01$; ***, $P < 0.001$ by Tukey's honestly significant difference (HSD) multiple-comparison test. (B) Effect on EPS production by the complementation of the wild-type strain or the Δ*ldhR* mutant by expressing in *trans* the *ldhRA* genes from pARG015-1 or the empty vector pBBR1MCS. Cells were incubated in the presence of the indicated sugars for 3 days at 37°C followed by EPS quantification. Significantly smaller amounts of EPS were produced when the *ldhRA* genes were overexpressed in both WT and mutant strains. *, $P < 0.05$; **, $P < 0.01$; ***, $P < 0.001$ by Tukey's HSD multiple-comparison test.

Deletion of *ldhR* has a positive effect on cell viability in glucose-rich medium. Due to the impairment of EPS production by *B. multivorans* ATCC 17616 in medium containing 2% D-glucose but not by the Δ*ldhR* mutant, we compared their growth and culture medium pH values in the presence of 2% D-mannitol or 2% D-glucose as the carbon source. No significant difference was observed in the exponential growth phases of both strains in mannitol-rich medium, although the final biomass of the Δ*ldhR* deletion mutant was consistently higher (Fig. 5A). The pHs of the culture media of both strains remained constant during the experiment. In medium with 2%

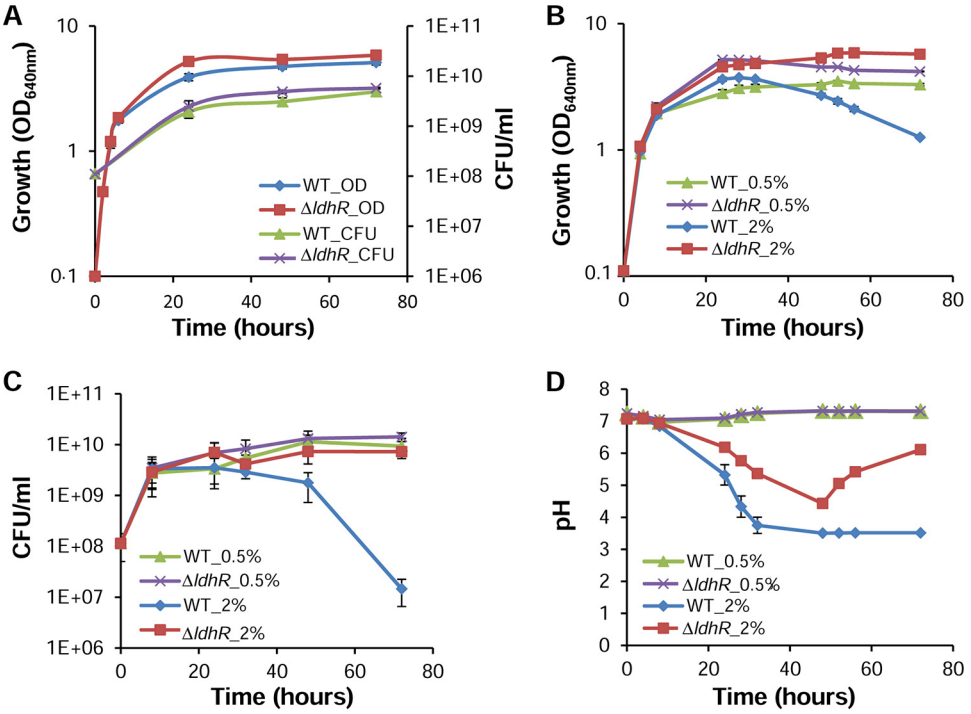

FIG 5 Loss of cell viability and medium acidification is dependent on the glucose concentration. Culture growth as measured by turbidity (OD_{640}) and CFU plating of *B. multivorans* ATCC 17616 and the Δ*ldhR* mutant grown for 72 h in the presence of 2% of D-mannitol (A) and 0.5% (B) or 2% (C) D-glucose. (D) Culture medium pH in the presence of D-glucose is shown. Error bars indicate the standard deviations.

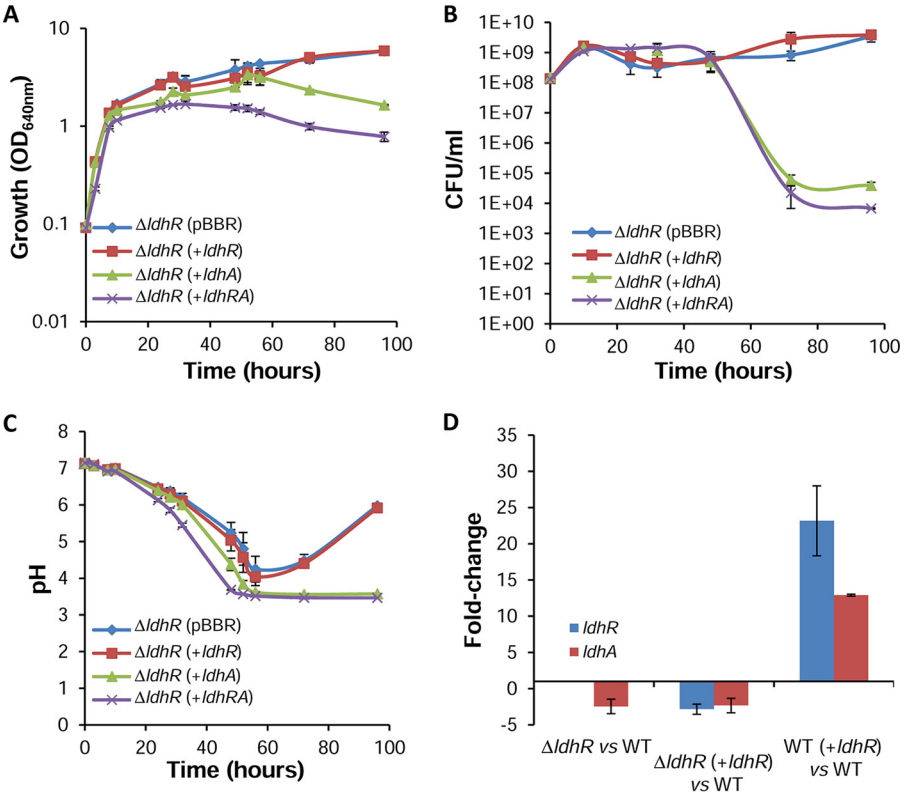

FIG 6 Complementation of the Δ*ldhR* mutant only rescues the wild-type growth properties in glucose-rich medium if *ldhA* is expressed alone or together with *ldhR*. Culture growth as measured by turbidity (OD_{640}) (A) and CFU (B) of the Δ*ldhR* mutant complemented with empty vector pBBR1MCS, pMM137-2 expressing *ldhR* from the *bce* promoter, pLM016-2 expressing *ldhA* from the *bce* promoter, and pARG015-1 expressing *ldhRA* genes from their own promoter. (C) Culture medium pH measured for the indicated strains. Genotype symbols are consistent for each panel. Cells were grown in medium supplemented with 2% D-glucose. (D) Quantitative RT-PCR analysis of transcript levels of *ldhR* and *ldhA* in the WT *B. multivorans* ATCC 17616, Δ*ldhR* mutant, and Δ*ldhR* mutant expressing *ldhR* from pMM137-2. Cells were grown in medium supplemented with D-glucose for 22 h at 37°C. Error bars indicate standard deviations.

D-glucose, both strains displayed similar growth rates, but when entering stationary phase, the WT culture showed a decrease in optical density (OD) (Fig. 5B) as well as cell viability as determined by CFU count (Fig. 5C). Since it is known that glucose metabolism can lead to medium acidification, we measured the pH of the growth medium during the course of the experiment. Up to 48 h, the pH of the culture medium dropped for both the WT and the Δ*ldhR* mutant, reaching pH 3.5 and pH 4.4, respectively. After that time, the medium pH of the WT culture remained at 3.5, whereas the culture medium pH reproducibly increased to 6.0 by day 3 for the Δ*ldhR* mutant (Fig. 5D). When 0.5% D-glucose was used, no significant differences in growth and viability were observed, despite the higher biomass of the Δ*ldhR* mutant (Fig. 5B and C). The culture medium pH also remained constant and at a neutral value (Fig. 5D).

Genetic complementation of the Δ*ldhR* mutant by expressing *ldhR* under the control of the *bce* promoter did not restore either the WT impaired cell viability in the presence of 2% D-glucose or the culture medium acidification to a pH of approximately 3.5 (Fig. 6A to C). This suggests lack of *ldhR* expression from the plasmid or a polarity effect of the trimethoprim resistance cassette on *ldhA* gene expression. To test these hypotheses, we performed quantitative RT-PCR. The data confirmed the expression of the *ldhR* gene in the complemented mutant, although the level was lower than that of the WT strain (Fig. 6D). Overexpression of *ldhR* in the WT strain also resulted in increased levels of *ldhR* expression, discarding the hypothesis of deficient expression from the *bce* promoter. Additionally, the expression of *ldhA* was decreased both in the Δ*ldhR* mutant and in the complemented mutant (Fig. 6D), confirming not only the polarity of the

trimethoprim resistance cassette on *ldhA* expression but also that the Δ*ldhR* mutant acts effectively as an *ldhRA* double mutant. Nevertheless, *ldhA* expression was increased when *ldhR* was overexpressed in the WT strain, giving additional support to the hypothesis that the *ldhR* and *ldhA* genes are in a polycistronic operon and confirming the direct or indirect involvement of the LdhR regulator in *ldhA* expression. Transcription data from *B. thailandensis* E264 show a 4.8-fold decreased expression of the *ldhA* gene when the upstream gene *scmR* was deleted (21), also supporting our observations in *B. multivorans* ATCC 17616.

In the Δ*ldhR* mutant, the overexpression of *ldhA* alone (pLM016-2) or together with *ldhR* restored the WT phenotype, with a decrease in optical density and cell viability and no recovery of the culture medium pH from 3.5 to 6 (Fig. 6A to C), confirming the involvement of LdhA protein in these phenotypes. The introduction of each of the three plasmids into the WT strain slightly enhanced the negative growth effects in the presence of 2% D-glucose, being more visible for the strain expressing *ldhRA* genes simultaneously (see Fig. S2A to C).

Taken together, our data show that the extreme acidification of the growth medium is possibly the cause of the decreased cell viability of WT cells in the presence of 2% D-glucose. This acidification is most likely due to organic acid secretion and, in particular, to the activity of the D-lactate dehydrogenase LdhA involved in the production of D-lactic acid from pyruvate.

Negative effect on cell viability and EPS production in glucose-rich medium is prevented by buffering the growth medium. To confirm that loss of cell viability is dependent on the observed acidic pH, we grew the WT and Δ*ldhR* mutant cells in medium supplemented with 2% D-glucose buffered with 0.2 M Tris-HCl with an initial pH of 7.2. Under these conditions, the WT and the Δ*ldhR* mutant showed similar growth trends and viability, although the Δ*ldhR* mutant exhibited a higher final biomass (see Fig. S3A and B). The acidification of the growth medium was also observed for both strains, but the lowest pH values obtained were 4.8 for the WT strain and 5.3 for the Δ*ldhR* mutant (Fig. S3C). After reaching this minimum, the culture medium pHs of both strains recovered toward neutrality. EPS production was also quantified after 96 h of growth in buffered 2% D-glucose-containing medium, with the WT strain recovering its ability to produce EPS, despite a reduction of 25% compared with that of the Δ*ldhR* mutant (Fig. S3D).

Cell survival threshold is surpassed by secretion of D-lactate. To examine whether the pH drop in glucose-rich medium was due to organic acid production, we employed reverse-phase high-pressure liquid chromatography (HPLC). By comparing peak retention times with standards, we identified the peaks corresponding to gluconate (GN), 2-ketogluconate (2KG), and D-lactate. In accordance with the pH drop by 48 h of growth in the presence of 2% D-glucose, both the WT and Δ*ldhR* mutant strains converted GN to 2KG, though the concentration was higher for the WT strain (Fig. 7A). In the following hours, the 2KG concentration decreased in the Δ*ldhR* mutant, most likely due to its consumption, while in the WT strain, the levels remained high and constant due to the loss of cell viability (Fig. 7A). An inspection of D-glucose consumption shows the same trend for both strains, with no detectable quantity by 48 h (Fig. 7B). D-Lactate increased in the growth medium of the WT strain up to 7 mM at 32 h, decreased to 5 mM until 48 h, and remained the same until the end of the experiment (Fig. 7B). From the Δ*ldhR* mutant supernatant, no D-lactate was detected.

The growth of the WT and the Δ*ldhR* mutant in 0.2 M Tris-buffered medium leads to similar consumption of D-glucose and its conversion to 2KG until 48 h, after which both strains are able to consume this metabolite at similar rates (data not shown). The D-lactate concentration increased in the growth medium of the WT strain up to 48 h, but then it was reduced by consumption, and at 72 h, no D-lactate was detected. From the Δ*ldhR* mutant supernatant, no D-lactate was detected. The overexpression of *ldhR* in the WT strain increased the concentration of D-lactate in the supernatant, possibly due to a positive effect on the expression of *ldhA* (Fig. S2D). When *ldhA* is expressed in the WT strain, the D-lactate concentration was even higher.

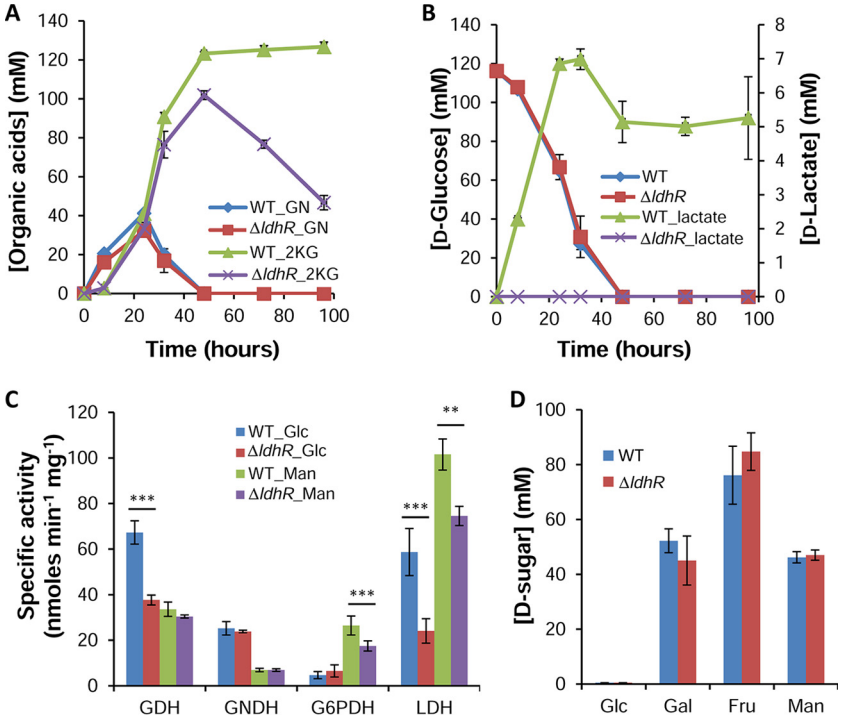

FIG 7 D-Lactate accumulation in the culture medium was only observed for the wild-type strain. (A and B) Concentration of the organic acids gluconate (GN) and 2-ketogluconate (2KG) (A) and of D-lactate (B, right scale) in the supernatants of *B. multivorans* ATCC 17616 wild-type cells and the Δ*ldhR* mutant in medium supplemented with 2% D-glucose as measured by HPLC. Glucose consumption is shown in panel B (left scale). (C) Levels of the enzymes glucose dehydrogenase (GDH), gluconate dehydrogenase (GNDH), glucose-6P dehydrogenase (G6PDH), and lactate dehydrogenase (LDH) in total extracts of the indicated strains grown for 20 h in S medium supplemented with 2% D-glucose or 2% D-mannitol. Significantly lower enzymatic activity was found for the *ldhRA* mutant compared with that from the WT strain. **, $P < 0.01$; ***, $P < 0.001$ by Tukey's HSD multiple-comparison test. (D) Sugar consumption at 48 h of growth by *B. multivorans* ATCC 17616 cells and the Δ*ldhR* mutant in medium supplemented with 2% (111 mM) D-sugar as measured by HPLC. Glc, D-glucose; Gal, D-galactose; Fru, D-fructose; Man, D-mannose. Error bars indicate the standard deviations.

Overall, D-glucose metabolism in the WT strain leads to organic acid secretion with a concomitant pH decrease, and if that value reaches a critical level, cells lose viability. By contrast, the absence of D-lactate accumulation by the Δ*ldhR* mutant prevents such stronger acidification, with cells remaining viable.

Enzymatic activities confirm organic acid secretion with the Δ*ldhR* mutant displaying lower lactate dehydrogenase activity than the WT strain. The data obtained for organic acid secretion by the WT strain and the Δ*ldhR* mutant were confirmed by measuring key enzymes from the direct oxidative and phosphorylative pathways of D-glucose dissimilation, as well as for the conversion of pyruvate into lactate. Cells were grown in the presence of 2% D-glucose or D-mannitol to measure the activation of one or the other pathway. In general, in the presence of D-glucose, the enzymes of the oxidative pathway (glucose dehydrogenase [GDH] and gluconate dehydrogenase [GNDH]) had higher specific activities than in D-mannitol-rich medium (Fig. 7C). Conversely, glucose-6-phosphate dehydrogenase (G6PDH) activity was higher in D-mannitol-rich medium. A comparison of the WT and the Δ*ldhR* mutant showed no difference in the enzymatic activities of the tested enzymes, except for lower activities of GDH and G6PDH in medium supplemented with D-glucose and D-mannitol, respectively, in the mutant (Fig. 7C). The measurement of total lactate dehydrogenase (LDH) activity in crude extracts revealed lower specific activity in the Δ*ldhR* mutant compared with that in the WT in both D-glucose and D-mannitol-rich media (Fig. 7C). This result confirms the involvement of D-lactate dehydrogenase LdhA in the WT cells' ability to convert pyruvate into D-lactate.

TABLE 1 Acidification of the culture medium and secretion and consumption of D-lactate as a consequence of 2% D-glucose dissimilation

Strain	Characteristic	Medium acidification/ maximal recovery (pH)	D-Lactate secretion/ consumption
B. multivorans JTC	Chronic granulomatous disease	4.0/6.3	Yes/yes
B. multivorans VC3161	Cystic fibrosis isolate	3.6/3.6	Yes/no
B. multivorans VC7495	Cystic fibrosis isolate	4.0/6.5	Yes/yes
B. multivorans VC6882	Cystic fibrosis isolate	4.9/6.3	Yes/yes
B. multivorans VC12539	Cystic fibrosis isolate	4.8/6.6	Yes/yes
B. multivorans VC8086	Cystic fibrosis isolate	4.8/6.6	Yes/yes
B. multivorans VC9159	Cystic fibrosis isolate	4.0/6.4	Yes/yes
B. multivorans VC12675	Cystic fibrosis isolate	4.9/6.2	Yes/yes
B. multivorans D2095	Cystic fibrosis isolate	3.5/3.5	Yes/no
B. ambifaria CEP0996	Cystic fibrosis isolate	5.1/6.7	Yes/yes
B. stabilis LMG 14294	Cystic fibrosis isolate	6.1/6.7	Yes/yes
B. anthina J2552	Rhizosphere	5.2/6.9	ND/NA[a]
B. dolosa CEP1010	Cystic fibrosis isolate	3.7/3.7	Yes/no
B. cenocepacia ATCC 17765	Urinary tract infection	6.3/7.1	Yes/yes
B. cenocepacia J2315	Cystic fibrosis isolate	6.5/6.5	ND/NA
B. cepacia ATCC 25416	*Allium cepa*	5.7/7.0	ND/NA
B. contaminans IST408	Cystic fibrosis isolate	4.5/5.9	ND/NA
B. vietnamiensis G4	Industrial waste treatment facility isolate	5.5/6.3	ND/NA

[a]ND, not detected; NA, not applicable.

Growth medium acidification depends on the metabolized sugar and is strain dependent. To test whether the involvement of LdhR in relieving carbon overflow was specific for D-glucose or also involved other sugars, we grew the WT and the Δ*ldhR* mutant in medium supplemented with other carbon sources. Growth in the presence of sugars metabolized by the phosphorylative pathway (Fig. 1), such as D-fructose and D-mannitol, resulted in no medium acidification for either of the tested strains, while D-mannose led to a slight pH decrease of the culture medium. No D-lactate, 2KG, or GN was detected either in the WT or in the Δ*ldhR* mutant (data not shown). The growth of the two strains in the presence of another sugar metabolized by the direct oxidative pathway (Fig. 1), such as D-galactose, led to culture medium pH acidification to a minimum of 5.2 in the WT strain and 5.5 in the Δ*ldhR* mutant at 48 h, with both strains recovering to pH neutrality by 72 h. D-Lactate was identified in the supernatant of the WT but not of the Δ*ldhR* mutant (data not shown). The consumption rates of the several sugars measured at 48 h of growth show that while D-glucose is depleted, for the other sugars, there is still a considerable amount of the initial concentration, and no significant differences were observed between the WT and the Δ*ldhR* mutant (Fig. 7D). These data show that metabolic overflow is caused only by the high D-glucose dissimilation rate.

Next, we tested whether the negative effect on cell survival registered in the presence of 2% D-glucose was unique for *B. multivorans* ATCC 17616 or if it was a more common phenomenon in the *B. cepacia* complex. Eighteen additional strains were tested to determine the minimum pH value reached in the culture medium and whether they recovered to higher pH values and if D-lactate was produced and consumed. The data shown in Table 1 indicate that only three strains (*B. multivorans* VC3161, *B. multivorans* D2095, and *B. dolosa* CEP1010) had results similar to those of *B. multivorans* ATCC 17616; namely, the culture medium pH decreased to 3.5 to 3.7 with no recovery and D-lactate was secreted but not consumed. A second group of 10 strains (*B. multivorans* strains JTC, VC7495, VC6882, VC12539, VC8086, VC9159, and VC12675, *B. ambifaria* CEP0996, *B. stabilis* LMG 14294, and *B. cenocepacia* ATCC 17765) showed minimum culture medium pH values ranging from 4.0 to 6.3, but these values increased toward neutrality. All these strains secreted D-lactate into the growth medium during the first 48 h, but it was consumed in the following hours. From the last group of five strains (*B. anthina* J2552, *B. cenocepacia* J2315, *B. cepacia* ATCC 25416, *B. contaminans* IST408, and *B. vietnamiensis* G4), we were unable to detect D-lactate, but the culture medium pH decreased to values ranging from 4.5 to 6.5 and then increased to neutrality (Table 1). Enzymatic activities of GDH, GNDH, G6PDH, and LDH in *B. dolosa* CEP1010 (51.7 ± 9.8, 16.0 ± 1.3, 11.2 ± 2.9, and 119.2 ± 12.5 nmol · min^{-1} · mg^{-1},

respectively) and in *B. cenocepacia* ATCC 17765 (15.5 ± 0.8, 5.0 ± 0.4, 52.6 ± 3.7, and 97.4 ± 8.8 nmol · min^{-1} · mg^{-1}, respectively) grown in medium with 2% D-glucose confirmed the differential use of both D-glucose dissimilation pathways. Altogether, these data suggest that most of the tested strains use the direct oxidative pathway for D-glucose utilization, but some might use the phosphorylative pathway only or a combination of both.

Growth in glucose-rich medium induces higher stress to WT than to Δ*ldhR* mutant cells. During the first 24 h of growth in medium containing 2% D-glucose, organic acid secretion by *B. multivorans* ATCC 17616 and the Δ*ldhR* mutant differed mainly by the presence of D-lactate in the WT culture medium, and consequently, a lower pH, and the absence of D-lactate in the mutant. To understand the physiological adaptations under these acidic conditions and identify genes that may be under the control of the LdhR regulator, we performed expression profiling studies. The transcriptomes of the Δ*ldhR* mutant and the WT strain grown in medium with 2% D-glucose were determined at 22 h of growth with the pH of the culture medium being 5.2 for the WT and 6.0 for the Δ*ldhR* mutant. A total of 132 genes were differentially expressed, 15 with increased expression and 117 with decreased expression (≥1.2-fold lower confidence bound change with a false discovery rate of ≤4.6%) (see Table S1).

Among the genes with increased expression in the mutant, we found *glnL* and *glnB-1*, encoding a signal transduction histidine kinase and the nitrogen regulatory protein P-II, respectively, as well as genes for the acquisition of inorganic nitrogen (*amt* and *narK*) and organic nitrogen (*urtA*) (Table 2). Genes encoding nitrogen assimilating enzymes, such as *nirB*, *nirD*, and *glnA*, were also upregulated in the mutant strain, suggesting higher needs of nitrogen for anabolic reactions. In comparison to that of the WT, the mutant strain is in a more favorable environment, since the culture medium is at a higher pH. That is reflected in the downregulation of many genes related to the stress response, RNA metabolism, and protein synthesis (Table 2). Regarding the stress response, we observed a downregulation of *rpoH*, encoding RNA polymerase factor sigma-32, as well as several genes encoding peptidases/proteases (Bmul_0546, *lon*, and *clpB*), heat shock proteins (Bmul_2055, Bmul_2056, Bmul_2384, *hslU*, and *grpE*), chaperones (*groEL*, *groES*, and *dnaK*), and *katE*, encoding catalase. Genes whose products are involved in synthesis (*rpoZ*, encoding the omega subunit of DNA-directed RNA polymerase) or degradation (*dnaK*, *groEL*, and *hfq2*) of RNA showed decreased expression in the Δ*ldhR* mutant. In the same line of evidence, 31 genes of ribosomal proteins, the *infC* gene encoding translation initiation factor IF-3, *thrS* encoding threonyl-tRNA synthetase, and *map* encoding a methionine aminopeptidase were downregulated in the mutant (Table S1). In terms of central metabolic pathways, few differentially expressed genes were found. Of relevance is the increased expression of *cydA* in the WT. This gene encodes the cytochrome *bd* ubiquinol oxidase subunit I, an enzyme less prone to inhibition by oxidative stress, enabling aerobic metabolism to continue under adverse conditions. Regarding secondary metabolism, there is a cluster of genes (*Bmul_5943* to *Bmul_5949*) whose expression was downregulated in the Δ*ldhR* mutant (Table 2). The products of these genes are homologous to methyltransferases, cytochrome P450, and Rieske [2Fe-2S] domain-containing proteins and might be required for the production of an unknown metabolite. Also of note is the decreased expression in the Δ*ldhR* mutant of adhesin BapA, which has been implicated in biofilm formation.

LdhR is required for planktonic cellular aggregate formation and adhesion to surfaces. During aerobic batch growth, we observed striking differences between the WT and the Δ*ldhR* mutant. After 72 h of growth in the presence of 0.5% or 2% of sugars such as D-glucose, D-galactose, D-fructose, D-mannitol, and D-mannose, we noticed the formation of macroscopic cellular aggregates by the WT strain *B. multivorans* ATCC 17616. These cellular aggregates could reach up to 2 to 3 mm in diameter after 3 days of growth. By contrast, the Δ*ldhR* mutant generated a more homogeneous cell suspension with occasional small aggregates (see Fig. S4A).

To determine when these planktonic cellular aggregates started to form, WT and Δ*ldhR* mutant strains were incubated in liquid medium containing 2% D-glucose for 24

TABLE 2 Set of genes differentially expressed between the Δ*ldhR* mutant and *B. multivorans* ATCC 17616 in medium supplemented with 2% D-glucose

Functional class	Gene identifier	LB-FC[a]	Gene name	Description
Regulatory genes	Bmul_0486	−1.3	*rpoH*	RNA polymerase factor sigma 32
	Bmul_1123	1.3	*glnL*	Signal transduction histidine kinase, N_2 specific, NtrB
	Bmul_1722	−1.3	*hfq2*	RNA chaperone Hfq
	Bmul_2393	−1.3	—[b]	Cold shock DNA-binding domain-containing protein
	Bmul_2400	−1.2	*rpoZ*	DNA-directed RNA polymerase, omega subunit
Nitrogen acquisition and assimilation	Bmul_0437	2.4	*glnB-1*	Nitrogen regulatory protein P-II
	Bmul_0438	1.4	*amt*	Ammonium transporter
	Bmul_1122	1.8	*glnA*	Glutamine synthetase, type I
	Bmul_1636	−1.4	*sbp*	ABC transporter periplasmic sulfate-binding protein
	Bmul_2482	1.4	*urtA*	Urea ABC transporter urea-binding protein
	Bmul_4146	1.3	*narK*	Major facilitator superfamily MFS_1
	Bmul_4147	1.7	*nirB*	Nitrite reductase (NADPH), large subunit
	Bmul_4148	2.0	*nirD*	Nitrite reductase (NADPH), small subunit
	Bmul_4149	1.3	*nos*	Molybdopterin oxidoreductase
Carbon metabolism and energy production	Bmul_2649	−1.9	—	Oxidoreductase flavin adenine dinucleotide (FAD)/ NADP-binding domain protein
	Bmul_3307	−1.4	*cydA*	Cytochrome *bd* ubiquinol oxidase subunit I
	Bmul_3795	2.2	—	TonB-dependent siderophore receptor
	Bmul_5321	−1.7	—	2-Amino-3-ketobutyrate coenzyme A ligase
Posttranslational modification, protein turnover, chaperones	Bmul_0546	−1.2	—	Peptidase M48 Ste24p
	Bmul_0776	−1.3	*clpS*	ATP-dependent Clp protease adaptor protein ClpS
	Bmul_1348	−1.2	*tig*	Trigger factor
	Bmul_1351	−1.3	*lon*	ATP-dependent protease La
	Bmul_1426	−1.3	*clpB*	ATP-dependent chaperone ClpB
	Bmul_2055	−1.5	—	Heat shock protein Hsp20
	Bmul_2056	−1.3	—	Heat shock protein Hsp20
	Bmul_2384	−1.4	—	Heat shock protein Hsp20
	Bmul_2528	−1.5	*groEL*	Chaperonin GroEL
	Bmul_2529	−1.6	*groES*	Chaperonin Cpn10
	Bmul_2633	−1.7	*dnaK*	Chaperone protein DnaK
	Bmul_2635	−1.4	*grpE*	Heat shock protein GrpE
	Bmul_3087	−1.3	*hslU*	ATP-dependent protease ATP-binding subunit HslU
Secondary metabolism	Bmul_5943	−1.4	—	Deoxyxylulose-5P synthase
	Bmul_5944	−1.4	—	Methyltransferase type 12
	Bmul_5945	−1.5	—	Methyltransferase type 12
	Bmul_5946	−1.6	—	Rieske [2Fe-2S] domain-containing protein
	Bmul_5947	−1.5	—	Hypothetical protein
	Bmul_5948	−1.4	—	Cytochrome P450
	Bmul_5949	−1.4	—	Rieske [2Fe-2S] domain-containing protein

[a]LB-FC, lower bound of fold change.
[b]—, not available.

h, and samples were analyzed by microscopy. Wild-type strain planktonic aggregates of different sizes were visible at 4 h of incubation (size range of 3 to 30 μm), and their number and sizes increased until the end of the experiment (size range, 50 to 1,000 μm) (Fig. 8A). By contrast, the Δ*ldhR* mutant was able to form aggregates by 24 h, but their size range was within 10 to 60 μm. Similar results were obtained for both strains when D-mannitol (not shown) or D-fructose was used in the growth medium (Fig. S4B).

To understand whether cellular aggregate formation is also dependent on the expression of the *ldhA* gene encoding a D-lactate dehydrogenase, the WT and the Δ*ldhR* mutant were complemented with *ldhR* or *ldhA* alone or simultaneously and grown in liquid medium containing D-mannitol. Microscopy of the aggregates formed by WT strains overexpressing each of the different genes showed dense aggregates with irregular surfaces and numerous ramifications (Fig. 8B). Planktonic aggregates formed by the Δ*ldhR* mutant with the empty vector or expressing *ldhR* alone were of a small size, but when *ldhA* was coexpressed with *ldhR*, aggregates with higher dimension and ramification values were evident (Fig. 8B). The expression of *ldhA* alone in the Δ*ldhR* mutant

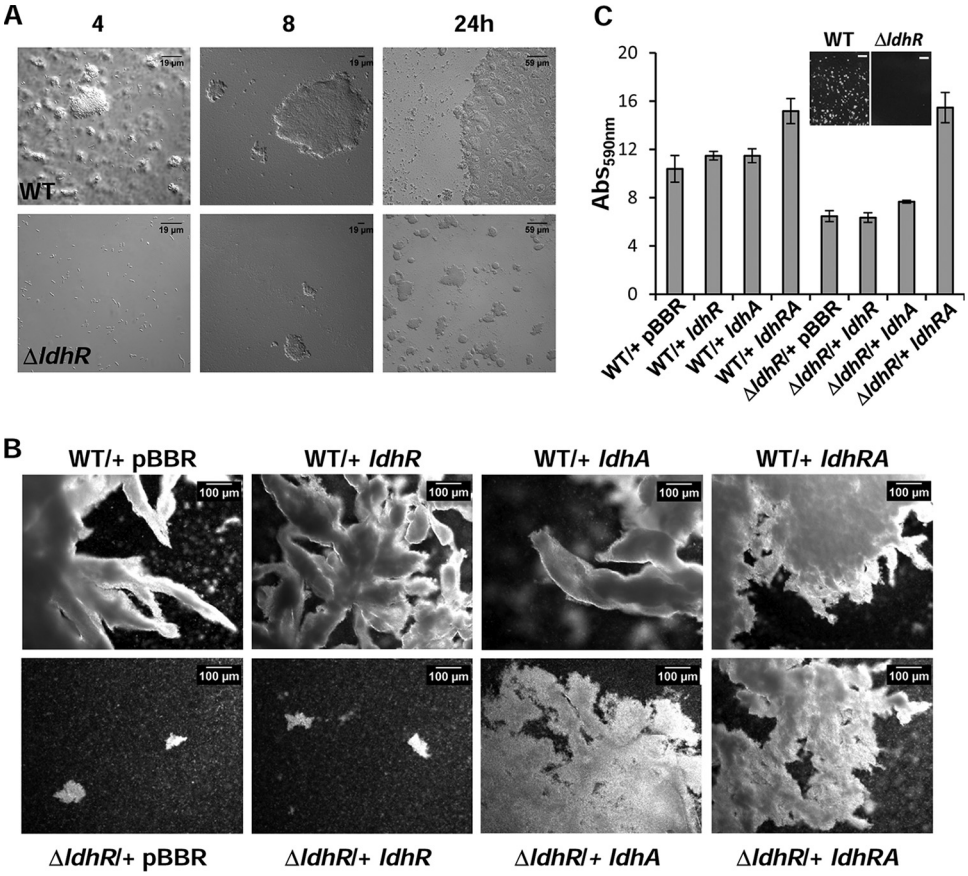

FIG 8 Planktonic cellular aggregate development and biofilm formation are dependent on LdhR and LdhA activities. (A) Images of planktonic aggregates formed during growth of *B. multivorans* ATCC 17616 wild-type cells and the Δ*ldhR* deletion mutant in medium supplemented with 2% D-mannitol for the indicated times. (B) Images of the planktonic cellular aggregates that sedimented after 5 min of static incubation of the indicated cultures grown for 72 h under constant agitation in medium containing 2% D-mannitol. (C) Images of biofilm cells attached to the solid surface of 24-well microtiter plates after 24 h of incubation with agitation in medium containing 2% D-mannitol, and biofilm quantification by the crystal violet staining method. Bars, 2.5 mm.

restored the formation of macroscopic cellular aggregates but in lower numbers than by complementation with *ldhRA*. This result suggests that planktonic cell aggregation also depends on *ldhA* gene product activity, but it is not the only determinant.

To evaluate whether adhesion to surfaces in the form of biofilms was also altered, the WT and the Δ*ldhR* mutant complemented with the several genes were grown in 24-well plates with agitation for 24 h in medium supplemented with D-mannitol. The results shown in Fig. 8C indicate that biofilm formation is approximately 40% lower in the Δ*ldhR* mutant than in the WT strain ($P < 0.001$). An image of the plastic surface before crystal violet staining shows macroscopic WT aggregates attached to the surface, while the Δ*ldhR* mutant formed a smooth surface (Fig. 8C). Complementation of the Δ*ldhR* mutant with *ldhA* produced a slight but statistically significant ($P < 0.05$) increase in biofilm formation, while complementation with both *ldhRA* genes recovered biofilm formation to levels even higher than in the WT strain. The overexpression of *ldhR* or *ldhA* alone in the WT strain produced a small increase in biofilm formation, but when both genes were expressed, this increase was 45% (Fig. 8C). Altogether, these results suggest that LdhR is relevant for surface-attached biofilm formation, and although the D-lactate dehydrogenase activity of LdhA contributes, it is not the only factor affecting biofilm formation.

Planktonic aggregate formation is a trait shared by several *B. cepacia* complex strains. To evaluate whether planktonic aggregates are common across members of the *B. cepacia* complex, we tested 74 additional strains from 9 different species, most

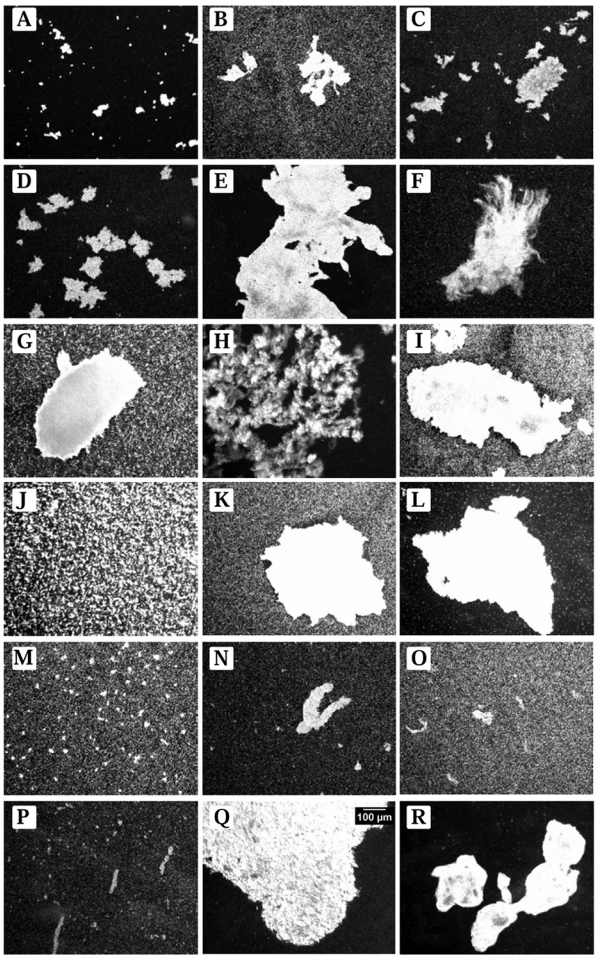

A- *B. cepacia* LMG 17997 UTI
B- *B. cepacia* FC1101 CF
C- *B. multivorans* CF-A1-1 CF
D- *B. multivorans* VC9159 CF
E- *B. multivorans* VC8086 CF
F- *B. multivorans* VC10037 CF
G- *B. cenocepacia* PC184 CF
H- *B. cenocepacia* CEP0571 CF
I- *B. cenocepacia* FC0447 CF
J- *B. stabilis* C7322 CF
K- *B. dolosa* CEP0021 CF
L- *B. vietnamiensis* FC0441 CGD
M- *B. contaminans* IST408 CF
N- *B. contaminans* strain E CF
O- *B. ambifaria* FC0168 CF
P- *B. ambifaria* CEP0958 CF
Q- *P. aeruginosa* FC1061 CF
R- *P. aeruginosa* 005 CF

Burkholderia species	With aggregates	Without aggregates
B. cepacia	3	4
B. multivorans	14	3
B. cenocepacia	8	6
B. stabilis	1	3
B. vietnamiensis	1	5
B. dolosa	1	4
B. ambifaria	4	1
B. anthina	0	4
B. contaminans	8	4

FIG 9 Planktonic growth of several strains from the *B. cepacia* complex leads to cellular aggregate formation. Light microscopy images of planktonic cellular aggregates obtained after 3 days of liquid batch cultures grown in medium supplemented with 2% D-mannitol (left panel) for the indicated strains. The bar shown in panel Q is the same for all other images. (Right, bottom) The number of isolates of each *B. cepacia* complex species analyzed and their ability to form planktonic cellular aggregates. UTI, urinary tract infection; CF, cystic fibrosis infection; CGD, chronic granulomatous disease.

of them isolated from CF patients' lung infections, and we included also 4 different *P. aeruginosa* strains. Microscopy revealed that 40 of 74 *Burkholderia* strains showed cellular aggregates larger than 10 μm when grown in medium containing 2% D-mannitol for 48 h with agitation (Fig. 9). The sizes and structures of the aggregates were variable and strain specific. *B. multivorans*, *B. ambifaria*, and *B. contaminans* had more strains that were able to form planktonic cellular aggregates. The four *P. aeruginosa* strains tested, all isolated from CF patients' infections, were also able to form cellular aggregates of different sizes (Fig. 9Q and R). The results from this analysis show that a considerable number of CF pathogens can grow as planktonic cellular aggregates in addition to as single cells.

Finally, to evaluate whether EPS plays a role in cellular aggregate formation, the mucoid *B. multivorans* VC5602 and a nonmucoid mutant derivative with a frameshift mutation in the *bceF* gene required for EPS biosynthesis were grown for 3 days in D-mannitol-rich medium. After inspecting the cultures, we found planktonic cellular aggregates in both strains, indicating that EPS was not relevant for cellular aggregate formation under the conditions tested.

DISCUSSION

This work presents the results from a functional analysis of the *B. multivorans* ATCC 17616 LdhR regulator and the D-lactate dehydrogenase LdhA. Despite ScmR and LdhA

from *B. thailandensis* E264 having the same genetic organization and high homology levels, there are striking differences between them. One important difference might be the dependence on quorum sensing (QS) to induce *scmR* (21) but not *ldhR* expression. Although we cannot exclude the possibility of *ldhR* expression being QS dependent, the lack of a *lux*-box sequence in the *ldhR* upstream region and the detection of D-lactate during the exponential growth phase give support to the idea of a lack of QS dependency of *ldhR* gene expression. Other striking differences are in the virulence and in biofilm formation. While ScmR represses virulence in *Caenorhabditis elegans* and biofilm formation (21), we found no differences between WT and the Δ*ldhR* mutant when infecting *Galleria mellonella* larvae (data not shown), and our observations implicate LdhR as an activator of biofilm formation. Furthermore, ScmR is both a repressor and activator of secondary metabolism (it regulates the synthesis of peptides, bacteriocins, and acids), while our transcriptomic data suggest LdhR is required for the expression of perhaps only one cluster of genes possibly involved in some unknown secondary metabolite production. Despite these differences between the regulatory networks controlled by the two regulators, both studies showed the upregulation of several genes involved in the stress response in WT cells. Altogether, our work and that of Mao and coworkers (21) show interesting examples of how subtle changes in regulatory and/or coding sequences of otherwise similar regulatory proteins can differentially affect the same phenotype, preventing general conclusions on their roles among different (but related) species.

Although *B. multivorans* LdhR does not seem to have as strong of an involvement in secondary metabolism as ScmR, it still has an important role in regulating carbon overflow, especially when D-glucose is used as the carbon source. The metabolism of D-glucose by *B. multivorans* ATCC 17616 (formerly *Pseudomonas cepacia* 249) was investigated previously (14). These authors estimated that the rate of dissimilation of glucose to gluconate and 2-ketogluconate via the direct oxidative pathway exceeds the rate of conversion of glucose to glucose-6P via the phosphorylative pathway by a factor of at least 12, concluding that the predominant route of glucose utilization in this strain is the direct oxidative pathway. Furthermore, they also reported culture medium acidification in the presence of D-glucose. Our data fully confirm these observations, but we further demonstrated that medium acidification is caused by the accumulation of gluconate, 2-ketogluconate, and D-lactate, and this strong pH decrease leads to the loss of cell survival. Similar to that with D-glucose, D-galactose utilization in *B. multivorans* ATCC 17616 also resulted in D-lactate secretion, but the culture medium pH never decreased below a critical level and cells were able to adapt and resume growth. The most likely explanation is the lower rate of D-galactose consumption than of D-glucose as shown in Fig. 7D.

Our data on the consumption of sugars, such as D-fructose and D-mannose, and the sugar alcohol D-mannitol by *B. multivorans* ATCC 17616 showed their dissimilation through the phosphorylative pathway. These compounds are transported across the plasma membrane and converted into fructose-6P prior to gluconate-6P formation and entering the Entner-Doudoroff pathway (Fig. 1). Possibly due to transport limitations and/or the enzymatic activity of the phosphorylative pathway enzymes, the consumption rate of these sugars is considerably lower than that of D-glucose. As a consequence, no accumulation of organic acids was detected, and the culture medium pH remained close to neutrality.

The role of LdhR, and especially of LdhA, in carbon overflow seems to be dependent on the sugar being consumed and on the dissimilation rate. The faster catabolism of D-glucose and D-galactose (to a lesser extent) by the Entner-Doudoroff pathway leads to the increased formation of glyceraldehyde-3P and pyruvate. To regenerate the NADH used in these reactions, pyruvate is converted into lactate (and possibly other acids), which is also secreted into the culture medium, further contributing to the extracellular acidification observed in the WT strain. In the absence of LdhR and consequently also the absence of D-lactate dehydrogenase LdhA activity (though there was still lactate dehydrogenase activity in the crude extracts), no secretion of D-lactate was observed, and the drop in pH was attenuated. The absence of carbon overflow

caused by the slower catabolism of sugars that use the phosphorylative pathway lowers the need for NADH regeneration, and LdhA might have a more limited role in regulating metabolic fluxes.

As we have shown, the growth of several strains from different species of the *B. cepacia* complex reveals a strain-dependent utilization of a pathway for D-glucose dissimilation. These differences might be caused mainly by the enzymatic activity of glucose dehydrogenase. Lessie and coworkers have shown that *B. multivorans* ATCC 17616 expresses the enzyme glucose dehydrogenase constitutively (23). Our analysis of enzymatic activity from the same strain and from *B. dolosa* CEP1010 confirmed this result. In addition, we observed that *B. cenocepacia* ATCC 17765, which has a much lower level of glucose dehydrogenase activity, has an increase of glucose-6P dehydrogenase activity and is most likely using the phosphorylative pathway for D-glucose dissimilation. These differences in D-glucose consumption might be relevant in an environment where several organisms compete for the same carbon sources. The fast conversion of glucose into less accessible compounds such as gluconate and 2-ketogluconate, together with the lowering of the surrounding pH, will certainly exclude some competitors. Another advantage is that protons generated from these oxidation steps contribute directly to transmembrane proton motive force and therefore to ATP synthesis (24).

The expression data showed that another side effect of organic acid secretion when cells are grown in an excess of D-glucose is the induction of a stress response, possibly against intracellular acidification. Since the pK_a values for D-lactate, gluconate, and 2-ketogluconate are 3.86, 3.39, and 2.67, respectively, a major cause of intracellular acidification might be the entrance of D-lactic acid. Our data show that cultures where the pH stayed above 4 (Table 1) were still able to survive and resume growth, but once the pH was below this value, cells lost viability rapidly. D-Lactate is a weak acid, which means that an increase of the undissociated form occurs with lowering of the pH. This undissociated form is capable of diffusing through the cell membrane, affecting its structure and causing intracellular acidification as the acid dissociates in the cytosol and releases protons. The pH of medium in which the Δ*ldhR* mutant is grown with an excess of D-glucose is lowered to 4.4, but this value seems to be harmless, because cells continue growing and eventually consume the organic acids. This different behavior is reflected in the transcriptomic data which confirms the stronger (although inefficient under our *in vitro* conditions) induction of stress response mechanisms, including increased expression in the WT of the gene encoding the heat shock response transcriptional regulator RpoH, as well as several genes encoding heat shock proteins, chaperones, and the proteases ClpB, ClpS, Lon, and HslU. An increased amount of these proteins in the cell would help to fold proteins and degrade the denatured ones. A study of the sigma factor RpoH1 in the regulation of *Sinorhizobium meliloti* genes upon pH stress also identified the differential expression of several RpoH1-dependent genes, including the upregulation of genes encoding heat shock proteins, such as IbpA, GrpE, GroEL5, and Hsp20, and proteases, such as ClpA, ClpB, ClpS1, ClpP2, ClpX, DegP1, Lon, and HslV, as well as the downregulation of genes involved in translation and nitrogen metabolism, such as NarB, NirB, NirD, and GlnK (25). The upregulation of stress response genes in the WT *B. thailandensis* E264 is attributed to the adaptation to stationary-phase growth (21). Yet, it cannot be excluded that this induction of stress response gene expression might result from the presence of high concentrations of toxic secondary metabolites in the culture medium.

One of the main findings implicates LdhR, and LdhA to a certain extent, in planktonic cellular aggregate formation. These aggregates are free-floating biofilm-like structures that do not require a surface to attach to. The growth of *P. aeruginosa* PAO1 in liquid batch cultures confirmed the preferential formation of planktonic cellular aggregates during the growth phase as opposed to free cells, but under stress conditions, such as the ones imposed by nutrient limitation, these aggregates disperse into single cells as reflected by an increase in optical density (20). In contrast to that with *P. aeruginosa*, we did not observe a sudden increase of optical density at the

beginning of the stationary phase, and the number/size of the *Burkholderia* aggregates continued to increase with time. Planktonic cellular aggregates are particularly relevant for bacteria infecting the CF lungs, as it has been shown that *P. aeruginosa* is found in lung tissues near the epithelial cell surface as non-surface-attached microcolonies (18). In another study that examined *P. aeruginosa*- and *B. cepacia* complex-infected CF lung tissues by immunostaining, *P. aeruginosa* was found in the form of microcolonies, while *B. cepacia* complex bacteria were found both as single cells and as cellular aggregates (2). At least two regulators have been shown to influence microcolony formation by *P. aeruginosa*. One of them is the LTTR BvlR whose inactivation prevented microcolony formation, but the mechanism is unknown (19). The other identified regulator is the two-component regulator MifR, with *mifR* mutant biofilms exhibiting thin structure-lacking microcolonies (17). This phenotype was dependent on pyruvate utilization, since the inactivation of genes encoding lactate dehydrogenase and aconitate hydratase abrogated microcolony formation in a manner similar to that from *mifR* inactivation, suggesting that the fermentation of pyruvate is required for microcolony formation. An explanation is that within microcolonies, *P. aeruginosa* cells experience oxygen-limiting but energy-rich conditions and use pyruvate fermentation as a means of redox balancing, allowing microcolony formation and biofilm development (17). The contribution of D-lactate dehydrogenase for *B. multivorans* ATCC 17616 planktonic aggregates and biofilm formation might also be due to the anoxic environment in the interior of the aggregate, inducing cells to ferment pyruvate as a means of redox balancing. Nevertheless, LdhA activity is not the only factor involved in the formation of cellular aggregates and biofilms, as shown by the partial complementation of these phenotypes by the mutant strain. Adhesin BapA might also contribute to the formation of these planktonic cell aggregates and biofilms, since its expression was upregulated in the WT strain. This adhesin has been implicated in *B. cenocepacia* microcolony formation, and its inactivation gave rise to a porous and disconnected biofilm (26). A study carried out with *B. thailandensis* showed a role of C_8-homoserine lactone in cell aggregation once a sufficient population number was reached, implicating quorum sensing in the self-aggregation phenotype (27). Further studies need to be conducted with *B. multivorans* to assess these possibilities.

Our data showing a high biofilm formation ability of the WT strain, with visible aggregates attached to the surface, in contrast to the smooth biofilm formed in smaller amounts by the Δ*ldhR* mutant, is in line with results from a study to determine the relative fitness of single cells and preformed aggregates during early development of *P. aeruginosa* biofilms, which showed a single-cell density-dependent fitness of the aggregates (28). These authors showed that when growth resources are abundant, aggregates have a disadvantage, because there is poor access to resources at the interior of the aggregate. However, if competition for resources is high, the aggregates have higher fitness because they can protrude above the surface and cells at the top of the aggregate have better access to growth resources. Another possible link between biofilm formation and the LdhR regulator was observed for an experimentally evolved *B. cenocepacia* HI2424 biofilm during 1,050 generations of selection (29). A mutation analysis revealed early beneficial mutations in the gene encoding the LdhR homologue (Bcen2424_0826), generating new haplotypes. Three different mutations were identified in the three ecotypes and consisted of a two-codon deletion and a single nucleotide polymorphism (SNP) (Δ38A, Δ39M, and L40V, respectively) which mapped to the DNA-binding domain (Fig. S1A). The effect of these mutations in the DNA-binding ability of the regulator and its effect on gene expression are unknown. These observed mutations might be beneficial for growth in the D-galactose minimal medium used in that study, but can also reflect selection for biofilm production.

The production of EPS, namely, cepacian, is a widespread trait in *B. cepacia* complex bacteria (6, 7). Although the genes encoding the proteins involved in cepacian biosynthesis are well known (5), the regulatory elements controlling the expression of this phenotype remain unknown. The exception is the regulator σ^{54}, which has been shown to positively regulate EPS production in *B. cenocepacia* grown under nitrogen starvation

(30). Here, we have shown a negative effect in EPS biosynthesis by LdhR and LdhA, but this might be a consequence of planktonic cellular aggregate formation. Cells of the Δ*ldhR* mutant grow as single cells and small aggregates, and most of them contribute to EPS production. By contrast, WT aggregates are much larger and possibly have smaller contributions to EPS biosynthesis, explaining the lower yield in the presence of carbon sources such as D-mannitol, D-mannose, and D-fructose. In addition to cell aggregation having an influence on EPS biosynthesis, we observed that EPS production does not seem to influence planktonic aggregate formation. Indeed, the EPS producer *B. multivorans* VC5602 and its isogenic mutant VC5602-nmv1 deficient in EPS due to a mutation in *bceF* both form aggregates, although we did not assess whether they are structurally similar. The downregulation of *ldhR* expression in nonmucoid isolates can be explained as the result of a genetic program for adaptation to different oxygen tensions. During growth in liquid medium, nonmucoid cells are not exposed to significantly limited oxygen diffusion, while the presence of EPS surrounding mucoid cells would create a somewhat less aerated environment. In this last circumstance, cells might sense some degree of oxygen limitation and induce alternative ways, such as pyruvate fermentation, to obtain energy.

Although *ldhR* or *ldhA* genes were not found to be mutated in serial isolates of *B. multivorans* and *B. dolosa* sampled from long-term CF lung infections (31, 32), a possible role for these genes in these persistent infections where oxygen gradients are present and fermentation is an alternative to obtain energy cannot be excluded. The observation that *B. cepacia* complex bacteria are also present in the mucus layer as cell aggregates (2) is an indication of the relevance of this type of growth, which possibly provides additional resistance against antimicrobials and the immune system. Planktonic cellular aggregate formation was also observed in almost all tested *B. cepacia* complex species and in more than 50% of the CF isolates analyzed. These are good indications for possible roles of LdhR and LdhA as persistence determinants, and more research into their function is needed.

In conclusion, we have shown that the LTTR LdhR and the D-lactate dehydrogenase LdhA are implicated in the formation of planktonic cellular aggregates and biofilms, properties possibly relevant in natural environments and within hosts. These cellular aggregates have decreased oxygen gradients toward the center, and fermentation of pyruvate would allow these cells to stay viable. We also showed the role of LdhA in the production of D-lactate to decrease the overflow of metabolic intermediates caused by dissimilation of excess sugars such as D-glucose and D-galactose. The fast catabolism of preferred carbon sources into organic acids is especially advantageous in natural environments. Overall, our findings evidence the important role of LdhR regulatory circuits in cells for adaptation to diverse environments.

MATERIALS AND METHODS

Bacterial strains and growth conditions. The bacterial strains and plasmids used in this study are described in Table 3. *E. coli* was grown at 37°C in Lennox broth (LB) with or without agar, supplemented with kanamycin (50 μg/ml), trimethoprim (50 μg/ml), or chloramphenicol (25 μg/ml) when required to maintain selective pressure. *Burkholderia* strains were grown at 37°C with 200 rpm of orbital agitation in LB or in S medium (12.5 g/liter $Na_2HPO_4{\cdot}2H_2O$, 3 g/liter KH_2PO_4, 1 g/liter K_2SO_4, 1 g/liter NaCl, 0.2 g/liter $MgSO_4{\cdot}7H_2O$, 0.01 g/liter $CaCl_2{\cdot}2H_2O$, 0.001 g/liter $FeSO_4{\cdot}7H_2O$, 1 g/liter yeast extract, 1 g/liter Casamino Acids, pH 7.2) (33) supplemented with 2% (wt/vol) of one of the following carbon sources: D-glucose, D-mannitol, D-galactose, D-mannose, or D-fructose. Growth medium for *B. multivorans* was supplemented with the following antibiotics: trimethoprim (100 μg/ml), ampicillin (100 μg/ml), and chloramphenicol (200 μg/ml).

DNA manipulation and cell transformation techniques. Genomic DNA from *Burkholderia* was extracted by using the DNeasy blood and tissue kit (Qiagen) according to the manufacturers' recommendations. Plasmid DNA isolation and purification, DNA restriction, agarose gel electrophoresis, DNA amplification by PCR, and *E. coli* transformation were performed using standard procedures (34). *Burkholderia* electrocompetent cells were transformed by electroporation using a Bio-Rad Gene Pulser II system (200 Ω, 25 μF, 2.5 kV) and grown overnight before being plated on selective medium. Triparental conjugation to *B. multivorans* strains was performed using the helper plasmid pRK2013.

Mutant construction. The 1,791-bp HindIII/XbaI upstream region of *ldhR* (*Bmul_2557*) was amplified by PCR from *B. multivorans* ATCC 17616 genomic DNA using the Bmul2557L primers (forward and reverse [fwd/rev]) (Table 4). After digestion with the appropriate restriction endonucleases, the fragment was cloned into a pBCKS vector giving rise to pAT312. The 1,800-bp XbaI/SacI downstream region of *ldhR* was

TABLE 3 Strains and plasmids used in this work

Strain or plasmid[a]	Relevant characteristic(s)	Source or reference
Strain		
B. multivorans ATCC 17616	Soil isolate, USA, EPS$^+$	43
B. multivorans Δ*ldhR*	ATCC 17616 derivative with *ldhR* replaced by a trimethoprim resistance cassette	This work
B. multivorans D2095	Cystic fibrosis isolate, Canada, EPS$^+$	16
B. multivorans D2095-nmv	Nonmucoid variant obtained under nutrient starvation, EPS$^-$	11
B. multivorans VC5602	Cystic fibrosis isolate, Canada, EPS$^+$	31
B. multivorans VC5602-nmv1	VC5602 derivative with a frameshift mutation in *bceF*, EPS$^-$	L. M. Moreira (unpublished)
B. multivorans CF-A1-1	Cystic fibrosis isolate, Canada	D. P. Speert
B. multivorans VC9159	Cystic fibrosis isolate, Canada	D. P. Speert
B. multivorans VC8086	Cystic fibrosis isolate, Canada	D. P. Speert
B. multivorans VC10037	Cystic fibrosis isolate, Canada	D. P. Speert
B. multivorans JTC	Chronic granulomatous disease, USA	44
B. multivorans VC3161	Cystic fibrosis isolate, Canada	D. P. Speert
B. multivorans VC7495	Cystic fibrosis isolate, Canada	D. P. Speert
B. multivorans VC6882	Cystic fibrosis isolate, Canada	D. P. Speert
B. multivorans VC12539	Cystic fibrosis isolate, Canada	D. P. Speert
B. multivorans VC12675	Cystic fibrosis isolate, Canada	D. P. Speert
B. contaminans IST408	Cystic fibrosis isolate, Portugal, EPS$^+$	45
B. contaminans IST408-nmv	Nonmucoid variant obtained under nutrient starvation, EPS$^-$	11
B. contaminans strain E	Cystic fibrosis isolate, Argentina	J. Degrossi
B. anthina FC0967	Cystic fibrosis isolate, Canada, EPS$^+$	D. P. Speert
B. anthina FC0967-nmv	Nonmucoid variant obtained under nutrient starvation, EPS$^-$	11
B. anthina J2552	Rhizosphere, UK	46
B. vietnamiensis PC259	Cystic fibrosis isolate, USA, EPS$^+$	47
B. vietnamiensis PC259-nmv	Nonmucoid variant obtained under nutrient starvation, EPS$^-$	11
B. vietnamiensis FC0441	Chronic granulomatous disease, Canada	D. P. Speert
B. vietnamiensis G4	Industrial waste treatment facility, USA	48
B. dolosa CEP0743	Cystic fibrosis isolate, Canada; EPS$^+$	D. P. Speert
B. dolosa CEP0743-nmv	Nonmucoid variant obtained under nutrient starvation, EPS$^-$	11
B. dolosa CEP0021	Cystic fibrosis isolate, Canada	D. P. Speert
B. dolosa CEP1010	Cystic fibrosis isolate, Canada	D. P. Speert
B. cepacia LMG 17997	Urinary tract infection, Sweden	44
B. cepacia FC1101	Cystic fibrosis isolate, Canada	D. P. Speert
B. cepacia ATCC 25416	*Allium cepa*, USA	44
B. cenocepacia PC184	Cystic fibrosis isolate, USA	49
B. cenocepacia CEP0571	Cystic fibrosis isolate, Canada	D. P. Speert
B. cenocepacia FC0447	Cystic fibrosis isolate, Canada	D. P. Speert
B. cenocepacia ATCC 17765	Urinary tract infection, UK	44
B. cenocepacia J2315	Cystic fibrosis isolate, UK	44
B. stabilis C7322	Cystic fibrosis isolate, Canada	D. P. Speert
B. stabilis LMG 14294	Cystic fibrosis isolate, Belgium	44
B. ambifaria FC0168	Cystic fibrosis isolate, Canada	D. P. Speert
B. ambifaria CEP0958	Cystic fibrosis isolate, Canada	D. P. Speert
B. ambifaria CEP0996	Cystic fibrosis isolate, Australia	46
P. aeruginosa FC1061	Cystic fibrosis isolate, Canada	D. P. Speert
P. aeruginosa 005	Cystic fibrosis isolate, Canada	D. P. Speert
Escherichia coli DH5α	DH5α *recA1* Δ(*lacZYA-argF*)*U169* ϕ80d*lacZ*ΔM15	Gibco BRL
Plasmid		
pRK2013	Tra$^+$ Mob$^+$ (RK2) Km::Tn*7* ColE1 origin, helper plasmid, Km^r	50
pBCKS	3.4-kb phagemid derived from pUC19, *lac* promoter, Cm^r	Stratagene
pUC-TP	pUC-GM derivative with a 1.1-kb Tp^r gene cassette, Ap^r Tp^r	51
pUK21	3089-bp pUC21 derivative, Km^r	52
pBBR1MCS	4,717-bp broad-host-range cloning vector, Cm^r	53
pAT312	pBCKS derivative containing the 1,719-bp HindIII/XbaI fragment upstream of *ldhR*	This work
pAT812	pAT312 derivative containing the 1,800-bp XbaI/SacI fragment downstream of *ldhR*	This work
pAT812-Tp	pAT812 derivative containing the trimethoprim resistance cassette	This work
pLM135-5	pUK21 derivative containing a 0.4-kb HindIII/NdeI fragment with the *bce* promoter region	45
pMM137-1	pLM135-5 derivative containing a 1,070-bp NdeI/XbaI fragment with *ldhR*	This work
pLM016-1	pLM135-5 derivative containing a 1,002-bp NdeI/XbaI fragment with *ldhA*	This work
pMM137-2	pBBR1MCS derivative containing the *bce* promoter and *ldhR* from pLM137-1	This work
pLM016-2	pBBR1MCS derivative containing the *bce* promoter and *ldhA* from pLM016-1	This work
pARG015-1	pBBR1MCS derivative containing a HindIII fragment expressing *ldhRA* from their own promoter	This work

[a]Due to the high number of strains tested in Fig. 9, only those forming planktonic cellular aggregates were included here. Tp^r, trimethoprim resistance; Cm^r, chloramphenicol resistance; Km^r, kanamycin resistance; Ap^r, ampicillin resistance; EPS$^+$, exopolysaccharide producer.

TABLE 4 List of primers used in this work

Primer set	Sequence[a]	
	Forward	Reverse
Bmul2557L	GAATCTAGACATGGTCTGAATCTGG	CCTAAGCTTGCTTCGAGATATGGC
Bmul2557R	AGCGAGCTCGTTCGAGCATCGGCTT	GACTCTAGACCGGGCCTGCAGTAAA
P1	GCAACATATGAACCAGATTCAGACCATG	TTGTCTAGAGTGAACGAATCGTCGTCGTA
P2	CATGCATATGCGCGTGATCCTGTTCAGC	CGTCTAGAGGCGTATCAGCGGCTC
P3	GCGAAGCTTGCGCGCGGATTGTG	AGGAAGCTTGCGGAAGGCCGAAG
2557/2558_RT	TCGAACATGCGATCGAGCACTT	TCGAGCGTGTCGTTGACGAA
2558/2559_RT	CTCGCGAACATCGAAGCGT	CGACGTGAAATGGCGCATGT
qRT_2557	CACTCGTCACGCGTTCGAT	GGTGGATCAGCCGCGTAT
qRT_2558	CGTGTTCGCGAAGATCATGA	TACGGCGGCATCGAATG
qRT_trpB	GACTGGGTCACGAACATCGAGAA	ACACCGAATGCGTCTCGATGA

[a]Restriction sites are underlined.

amplified using the Bmul2557R (fwd/rev) primers and cloned into the same restriction sites of pAT312, and the resulting plasmid was named pAT812. A fragment containing the trimethoprim resistance cassette from pUC-TP was then cloned into the XbaI site of pAT812, originating pAT812-Tp. To delete the *ldhR* from *B. multivorans* ATCC 17616, pAT812-Tp was introduced into this strain by electroporation. Recombinant colonies were first selected in the presence of trimethoprim and counter-selected in a medium supplemented with chloramphenicol. Gene deletion was confirmed by PCR amplification followed by DNA sequence determination.

Complementation assays. A 1,070-kb NdeI/XbaI fragment containing *ldhR* was amplified by PCR from *B. multivorans* ATCC 17616 genomic DNA using P1 primers (fwd/rev) (Table 4). The fragment was cloned into the NdeI/XbaI restriction sites of pLM135-5, a pUK21-derivative plasmid carrying 0.4 kb containing the *bce* promoter region directing the expression of the *bce* operon required for cepacian biosynthesis. The resulting pMM137-1 intermediate plasmid was digested with HindIII and XbaI, and the 1.47-kb fragment containing the *bce* promoter and *ldhR* gene was cloned into vector pBBR1MCS, resulting in plasmid pMM137-2 (Table 3). The same strategy was used to clone the *ldhA* gene (amplified with P2 [fwd/rev] primers) under the control of the *bce* promoter, resulting in plasmids pLM016-1 and the final pLM016-2. To clone the *ldhRA* genes under the control of their own promoters, a 2.7-kb fragment of the *B. multivorans* ATCC 17616 genome containing the upstream region of *ldhR* and the coding sequences of *ldhR* and *ldhA* was amplified by PCR using P3 (fwd/rev) primers. The amplified DNA was restriction digested with HindIII and ligated to pBBR1MCS, originating plasmid pARG015-1 (Table 3). After *E. coli* DH5α transformation and clone selection, the inserted genes were confirmed by DNA sequence determination. Plasmids pMM137-2, pLM016-2, and pARG015-1 were mobilized into *B. multivorans* ATCC 17616 and the Δ*ldhR* mutant by triparental conjugation. Transformants were selected on LB plates supplemented with 100 μg/ml of ampicillin and 200 μg/ml of chloramphenicol.

Isolation of RNA samples. For reverse transcription-quantitative PCR (qRT-PCR) and microarray analyses, cells were grown in S medium with 2% D-mannitol or D-glucose for 22 h at 37°C. For reverse transcription-PCR, cells were grown for 18 h in S medium supplemented with 2% D-mannitol under the same conditions. Three biological replicates were obtained for each tested strain. For RNA analysis, bacterial cells were resuspended in RNAprotect bacteria reagent (Qiagen), and total RNA extraction was carried out using the RNeasy mini kit (Qiagen) according to the manufacturer's recommendations. RNA was treated with DNase (RNase-free DNase; Qiagen) for 1 h at room temperature according to the manufacturer's protocol, and total RNA concentration was assessed using a NanoDrop ND-1000 spectrophotometer. RNA integrity for microarray analysis was checked on an Agilent 2100 Bioanalyzer using an RNA Nano assay.

Quantitative real-time RT-PCR. Total RNA was used in a reverse transcription reaction with TaqMan reverse transcription reagents (Applied Biosystems). qRT-PCR amplification of genes *ldhR*, *ldhA*, and *trpB* (for primer sequences, see Table 4) was performed with a model 7500 thermocycler (Applied Biosystems). The expression ratio of the target genes relative to the reference gene *trpB*, which showed no variation in transcription abundance under the conditions tested, was determined. The relative quantification of gene expression by real-time qRT-PCR was determined using the $\Delta\Delta C_T$ method (35).

Reverse transcription-PCR. To determine whether *ldhR* and *ldhA* are cotranscribed, a semiquantitative RT-PCR was performed. Total RNA was extracted from *B. multivorans* ATCC 17616 grown in S medium supplemented with D-mannitol for 18 h at 37°C with shaking at 200 rpm. A total of 200 ng of total RNA was used for reverse-transcription reactions using TaqMan reagent kits (Applied Biosystems, Roche). Synthesized cDNA was used as the template for 25-μl PCR mixtures with 0.2 μM primers 2557/2558_RT or 2558/2559_RT (Table 4), 0.2 mM deoxynucleosides triphosphate, 1.6 mM $MgSO_4$, 1× PCR amplification buffer, and 2.5 U of *Taq* polymerase (Bioline). Amplification occurred by an initial denaturation at 95°C for 5 min, 30 cycles of 30 s at 95°C, 45 s at 52°C, and 30 s at 72°C, and a final extension at 72°C for 10 min.

Processing of RNA samples for transcriptomic analysis. Total RNA was processed for use on Affymetrix custom *Burkholderia* arrays, according to the manufacturer's prokaryotic target preparation assay as described previously (16). Biological triplicates of RNA from each bacterial culture were processed and analyzed.

Microarray analysis. Scanned arrays were analyzed with Affymetrix Expression Console software to guarantee that all quality parameters were in the recommended range. Subsequent analysis was performed with DNA-Chip analyzer 2008. Since the custom arrays used represent two different *Burkholderia* species (16), a digital mask was applied leaving only the 9,610 probe sets representing *B. multivorans* ATCC 17616 transcripts for analysis. Then, the 6 arrays were normalized to a baseline array with median CEL intensity by applying an invariant set normalization method (36). Normalized CEL intensities of the arrays were used to obtain model-based gene expression indices based on a perfect match (PM)-only model (37). Replicate data (triplicates) for each bacterial isolate were weighted gene-wise using inverse squared standard error as the weights. All genes compared were considered to be differentially expressed if the 90% lower confidence bound of the fold change (LCB) between the experiment and baseline was above 1.2. The lower confidence bound criterion meant that we could be 90% confident that the fold change was a value between the lower confidence bound and a variable upper confidence bound. Li and Wong have shown that the lower confidence bound is a conservative estimate of the fold change and therefore more reliable as a ranking statistic for changes in gene expression (36).

Exopolysaccharide quantification. The amount of EPS was assessed based on the dry weight of the ethanol-precipitated polysaccharides recovered from triplicates of 100-ml culture samples of the different strains grown in liquid S medium supplemented with 2% (wt/vol) of different sugars over 3 days at 37°C with 200 rpm of orbital agitation as previously described (33).

Determination of carbon source and organic acid concentration in the culture medium. The supernatant of each culture (2 ml) was obtained by centrifugation at 14,000 × *g* for 10 min followed by filtration through a 0.2-μm-pore-size Whatman membrane filter. Carbon source consumption and organic acid production were monitored by HPLC using an Aminex HPX-87H (Bio-Rad) ion-exchange chromatography column, with elution at 65°C with 5 mM H_2SO_4 at a flow rate of 0.6 ml/min for 30 min and detection by UV-visible (UV-Vis) and refractive index (RI) detectors. The linearity of the method was tested, and concentrations were estimated based on calibration curves.

Preparation of bacterial extracts and enzyme assays. Bacteria were grown in 50 ml of S medium supplemented with 2% D-glucose or D-mannitol at 37°C for 20 h, and cells were collected by centrifugation. After being washed, pellets were stored at −80°C until used. Thawed cells were then suspended in 20 mM phosphate buffer (pH 6.8) and disrupted by sonication for 8 cycles of 30 s. For assays of glucose or gluconate dehydrogenase, lysates were supplemented with 1% (vol/vol) Triton X-100. The lysates were then centrifuged for 30 min at 12,000 × *g*, and supernatant fractions were immediately assayed for enzyme activities.

In vitro activities of D-glucose and D-gluconate dehydrogenases (EC 1.1.5.2 and EC 1.1.99.3, respectively) were measured at 37°C by monitoring the glucose or gluconate-dependent reduction of 0.3 mM 2,6-dichlorophenol indophenol (DCPIP) by following the decrease in absorbance of the assay mixtures at 600 nm with a spectrophotometer (UV-1700: PharmaSpec, Shimadzu). Reaction mixtures contained 150 mM phosphate buffer (pH 6.8), 10 mM D-glucose (or sodium D-gluconate), 0.3 mM phenazine methosulfate (PMS), and bacterial protein extract as described previously (13). The enzyme activity was calculated using an extinction coefficient of 20,600 $M^{-1} \cdot cm^{-1}$ for DCPIP. Activity of glucose-6-phosphate dehydrogenase (G6PDH) (EC 1.1.1.49) was determined at 37°C by monitoring substrate-dependent formation of NADH in reaction mixtures at 340 nm. Reaction mixtures contained 200 mM Tris-HCl (pH 8.5), 0.5 mM NAD^+, 10 mM glucose-6-phosphate, and bacterial protein extract. The enzyme activity was calculated using an extinction coefficient of 6,220 $M^{-1} \cdot cm^{-1}$ for NADH. The total activity of lactate dehydrogenase was determined at 37°C by monitoring the oxidation of NADH at 340 nm in the presence of sodium pyruvate. Reaction mixtures contained 50 mM 3-(*N*-morpholino)propanesulfonic acid (MOPS; pH 7.0), 0.12 mM NADH, 20 mM sodium pyruvate, and bacterial protein extract. One unit was defined as the amount of enzyme converting 1 nmol of substrate per minute. Protein concentrations were determined using the Bradford method (Bio-Rad reagent), using bovine serum albumin as a standard protein. Enzymatic activities were determined from two biological replicates, and each reaction was performed five times.

Microscopy analysis. *B. multivorans* ATCC 17616 and the Δ*ldhR* deletion mutant with/without complementation were grown for up to 72 h in S medium supplemented with D-glucose or D-mannitol. Images were acquired on a commercial Leica high content screening microscope, based on a Leica DMI6000 equipped with a Hamamatsu Flash 4.0 LT scientific complementary metal-oxide semiconductor (sCMOS) camera, using a 10× 0.3-numerical aperture (NA) objective, and controlled with the Leica LAS X software (Fig. 8A; see also Fig. S4B in the supplemental material), or a Zeiss Axioplan equipped with a Photometrics CoolSNAP fx camera, using a 10× 0.3-NA objective and controlled with software MetaMorph version 4.6r9 (Fig. 8B and Fig. 9) or a Pentax *ist DS digital camera (Fig. 8C; see also Fig. S4A). Cellular aggregate size was estimated with a ruler incorporated in the analysis software (Adobe Photoshop CS5) from at least 50 measures. Due to the weight of the coverslip, the aggregates are flattened.

Adhesion to surfaces and biofilm formation. To elucidate the role of *ldhR* in biofilm formation, cells were grown in a 24-well plate system modified from the procedure of Caiazza and O'Toole (38). Briefly, overnight cultures were adjusted to an optical density at 600 nm (OD_{600}) of 0.1 in fresh S medium supplemented with 2% D-mannitol and 100 μg/ml chloramphenicol and grown at 37°C with shaking at 200 rpm in 24-well microtiter plates (Orange Scientific) at a 45° angle, ensuring that the air-liquid interface crossed the centers of the flat-bottomed wells. After 24 h, cell cultures were removed and wells were washed three times with saline buffer and stained for 15 min with crystal violet (1% solution). After washing, the extent of biofilm formation was quantified as previously described (33).

***In silico* analysis of nucleotide and amino acid sequences.** The algorithm BLAST (39) was used to compare sequences of the deduced LdhR and LdhA amino acids to database sequences available at the National Center for Biotechnology Information (NCBI) or the Burkholderia Genome Database (http://www.burkholderia.com/bgd) (40). Alignments were performed using the program ClustalW (41). Molecular evolutionary relationships between LdhA and its homologues were determined using full-length protein sequences of all 185 members of the D-isomer-specific 2-hydroxyacid dehydrogenase family (PROSITE documentation entry PDOC00063; last updated April 2006). Analyses were conducted using the software package MEGA version 6.0 (42) which uses ClustalW for alignment and a neighbor-joining method for tree construction.

Statistical analysis. All quantitative data were obtained from at least three independent assays with two biological replicates. Error propagation was used to calculate standard errors, and one-way analysis of variance (ANOVA) and Tukey's multiple-comparison test were performed to assess statistical significance. Differences were considered statistically significant if the *P* value was lower than 0.05.

Ethics statement. The bacterial clinical isolates are from anonymous patients, and none of them were taken specifically for this study.

Accession number(s). Microarray data were deposited in the Gene Expression Omnibus (GEO) repository at NCBI under accession number GSE97006.

SUPPLEMENTAL MATERIAL

Supplemental material for this article may be found at https://doi.org/10.1128/AEM.01343-17.

SUPPLEMENTAL FILE 1, PDF file, 0.8 MB.

SUPPLEMENTAL FILE 2, XLSX file, 0.1 MB.

ACKNOWLEDGMENTS

We thank Mário R. Santos from Instituto Gulbenkian de Ciência, Oeiras (IGC), Portugal, for technical assistance with microscopy analysis. Microarrays were processed at the IGC's Gene Expression Unit.

This work was supported by Programa Operacional Regional de Lisboa 2020 (LISBOA-01-0145-FEDER-007317), Fundação para a Ciência e a Tecnologia, Portugal (PTDC/QUI-BIQ/118260/2010, UID/BIO/04565/2013), and a postdoctoral grant (SFRH/BPD/86475/2012) to I.N.S.

REFERENCES

1. Lipuma JJ. 2010. The changing microbial epidemiology in cystic fibrosis. Clin Microbiol Rev 23:299–323. https://doi.org/10.1128/CMR.00068-09.
2. Schwab U, Abdullah LH, Perlmutt OS, Albert D, Davis CW, Arnold RR, Yankaskas JR, Gilligan P, Neubauer H, Randell SH, Boucher RC. 2014. Localization of *Burkholderia cepacia* complex bacteria in cystic fibrosis lungs and interactions with *Pseudomonas aeruginosa* in hypoxic mucus. Infect Immun 82:4729–4745. https://doi.org/10.1128/IAI.01876-14.
3. Mahenthiralingam E, Urban TA, Goldberg JB. 2005. The multifarious, multireplicon *Burkholderia cepacia* complex. Nat Rev Microbiol 3:144–156. https://doi.org/10.1038/nrmicro1085.
4. Leitão JH, Sousa SA, Ferreira AS, Ramos CG, Silva IN, Moreira LM. 2010. Pathogenicity, virulence factors, and strategies to fight against *Burkholderia cepacia* complex pathogens and related species. Appl Microbiol Biotechnol 87:31–40. https://doi.org/10.1007/s00253-010-2528-0.
5. Ferreira AS, Silva IN, Oliveira VH, Cunha R, Moreira LM. 2011. Insights into the role of extracellular polysaccharides in *Burkholderia* adaptation to different environments. Front Cell Infect Microbiol 1:16. https://doi.org/10.3389/fcimb.2011.00016.
6. Zlosnik JE, Hird TJ, Fraenkel MC, Moreira LM, Henry DA, Speert DP. 2008. Differential mucoid exopolysaccharide production by members of the *Burkholderia cepacia* complex. J Clin Microbiol 46:1470–1473. https://doi.org/10.1128/JCM.02273-07.
7. Ferreira AS, Leitão JH, Silva IN, Pinheiro PF, Sousa SA, Ramos CG, Moreira LM. 2010. Distribution of cepacian biosynthesis genes among environmental and clinical *Burkholderia* strains and role of cepacian exopolysaccharide in resistance to stress conditions. Appl Environ Microbiol 76:441–450. https://doi.org/10.1128/AEM.01828-09.
8. Cunha MV, Sousa SA, Leitão JH, Moreira LM, Videira PA, Sá-Correia I. 2004. Studies on the involvement of the exopolysaccharide produced by cystic fibrosis-associated isolates of the *Burkholderia cepacia* complex in biofilm formation and in persistence of respiratory infections. J Clin Microbiol 42:3052–3058. https://doi.org/10.1128/JCM.42.7.3052-3058.2004.
9. Bylund J, Burgess LA, Cescutti P, Ernst RK, Speert DP. 2006. Exopolysaccharides from *Burkholderia cenocepacia* inhibit neutrophil chemotaxis and scavenge reactive oxygen species. J Biol Chem 281:2526–2532. https://doi.org/10.1074/jbc.M510692200.
10. Conway BA, Chu KK, Bylund J, Altman E, Speert DP. 2004. Production of exopolysaccharide by *Burkholderia cenocepacia* results in altered cell-surface interactions and altered bacterial clearance in mice. J Infect Dis 190:957–966. https://doi.org/10.1086/423141.
11. Silva IN, Tavares AC, Ferreira AS, Moreira LM. 2013. Stress conditions triggering mucoid morphotype variation in *Burkholderia* species and effect on virulence in *Galleria mellonella* and biofilm formation *in vitro*. PLoS One 8:e82522. https://doi.org/10.1371/journal.pone.0082522.
12. Sousa SA, Ulrich M, Bragonzi A, Burke M, Worlitzsch D, Leitão JH, Meisner C, Eberl L, Sá-Correia I, Döring G. 2007. Virulence of *Burkholderia cepacia* complex strains in gp91$^{phox-/-}$ mice. Cell Microbiol 9:2817–2825. https://doi.org/10.1111/j.1462-5822.2007.00998.x.
13. Sage A, Linker A, Evans LR, Lessie TG. 1990. Hexose phosphate metabolism and exopolysaccharide formation in *Pseudomonas cepacia*. Curr Microbiol 20:191–198. https://doi.org/10.1007/BF02091996.
14. Berka TR, Allenza P, Lessie TG. 1984. Hyperinduction of enzymes of the phosphorylative pathway of glucose dissimilation in *Pseudomonas cepacia*. Curr Microbiol 11:143–148. https://doi.org/10.1007/BF01567339.
15. Moreira LM, Videira PA, Sousa SA, Leitão JH, Cunha MV, Sá-Correia I. 2003. Identification and physical organization of the gene cluster involved in the biosynthesis of *Burkholderia cepacia* complex exopolysaccharide. Biochem Biophys Res Commun 312:323–333. https://doi.org/10.1016/j.bbrc.2003.10.118.
16. Silva IN, Ferreira AS, Becker JD, Zlosnik JEA, Speert DP, He J, Mil-Homens D, Moreira LM. 2011. Mucoid morphotype variation of *Burkholderia multivorans* during chronic cystic fibrosis lung infection is correlated with changes in metabolism, motility, biofilm formation and virulence. Microbiology 157:3124–3137. https://doi.org/10.1099/mic.0.050989-0.
17. Petrova OE, Schurr JR, Schurr MJ, Sauer K. 2012. Microcolony formation by the opportunistic pathogen *Pseudomonas aeruginosa* requires pyru-

vate and pyruvate fermentation. Mol Microbiol 86:819–835. https://doi.org/10.1111/mmi.12018.
18. Worlitzsch D, Tarran R, Ulrich M, Schwab U, Cekici A, Meyer KC, Birrer P, Bellon G, Berger J, Weiss T, Botzenhart K, Yankaskas JR, Randell S, Boucher RC, Döring G. 2002. Effects of reduced mucus oxygen concentration in airway *Pseudomonas* infections of cystic fibrosis patients. J Clin Invest 109:317–325. https://doi.org/10.1172/JCI0213870.
19. McCarthy RR, Mooij MJ, Reen FJ, Lesouhaitier O, O'Gara F. 2014. A new regulator of pathogenicity (*bvlR*) is required for full virulence and tight microcolony formation in *Pseudomonas aeruginosa*. Microbiology 160:1488–1500. https://doi.org/10.1099/mic.0.075291-0.
20. Schleheck D, Barraud N, Klebensberger J, Webb JS, McDougald D, Rice SA, Kjelleberg S. 2009. *Pseudomonas aeruginosa* PAO1 preferentially grows as aggregates in liquid batch cultures and disperses upon starvation. PLoS One 4:e5513. https://doi.org/10.1371/journal.pone.0005513.
21. Mao D, Bushin LB, Moon K, Wu Y, Seyedsayamdost MR. 2017. Discovery of *scmR* as a global regulator of secondary metabolism and virulence in *Burkholderia thailandensis* E264. Proc Natl Acad Sci U S A 114:E2920–E2928. https://doi.org/10.1073/pnas.1619529114.
22. Sainsbury S, Lane LA, Ren J, Gilbert RJ, Saunders NJ, Robinson CV, Stuart DI, Owens RJ. 2009. The structure of CrgA from *Neisseria meningitidis* reveals a new octameric assembly state for LysR transcriptional regulators. Nucleic Acids Res 37:4545–4558. https://doi.org/10.1093/nar/gkp445.
23. Lessie TG, Berka T, Zamanigian S. 1979. *Pseudomonas cepacia* mutants blocked in the direct oxidative pathway of glucose degradation. J Bacteriol 139:323–325.
24. Latrach Tlemçani L, Corroler D, Barillier D, Mosrati R. 2008. Physiological states and energetic adaptation during growth of *Pseudomonas putida* mt-2 on glucose. Arch Microbiol 190:141–150. https://doi.org/10.1007/s00203-008-0380-8.
25. de Lucena DKC, Pühler A, Weidner S. 2010. The role of sigma factor RpoH1 in the pH stress response of *Sinorhizobium meliloti*. BMC Microbiol 10:265. https://doi.org/10.1186/1471-2180-10-265.
26. Inhülsen S, Aguilar C, Schmid N, Suppiger A, Riedel K, Eberl L. 2012. Identification of functions linking quorum sensing with biofilm formation in *Burkholderia cenocepacia* H111. Microbiologyopen 1:225–242. https://doi.org/10.1002/mbo3.24.
27. Chandler JR, Duerkop BA, Hinz A, West TE, Herman JP, Churchill MEA, Skerrett SJ, Greenberg EP. 2009. Mutational analysis of *Burkholderia thailandensis* quorum sensing and self-aggregation. J Bacteriol 191:5901–5909. https://doi.org/10.1128/JB.00591-09.
28. Kragh KN, Hutchison JB, Melaugh G, Rodesney C, Roberts AEL, Irie Y, Jensen PØ, Diggle SP, Allen RJ, Gordon V, Bjarnsholt T. 2016. Role of multicellular aggregates in biofilm formation. mBio 7:e00237. https://doi.org/10.1128/mBio.00237-16.
29. Traverse CC, Mayo-Smith LM, Poltak SR, Cooper VS. 2013. Tangled bank of experimentally evolved *Burkholderia* biofilms reflects selection during chronic infections. Proc Natl Acad Sci U S A 110:E250–E259. https://doi.org/10.1073/pnas.1207025110.
30. Lardi M, Aguilar C, Pedrioli A, Omasits U, Suppiger A, Cárcamo-Oyarce G, Schmid N, Ahrens CH, Eberl L, Pessi G. 2015. σ^{54}-Dependent response to nitrogen limitation and virulence in *Burkholderia cenocepacia* strain H111. Appl Environ Microbiol 81:4077–4089. https://doi.org/10.1128/AEM.00694-15.
31. Silva IN, Santos PM, Santos MR, Zlosnik JEA, Speert DP, Buskirk SW, Bruger EL, Waters CM, Cooper VS, Moreira LM. 2016. Long-term evolution of *Burkholderia multivorans* during a chronic cystic fibrosis infection reveals shifting forces of selection. mSystems 1:e00029-16. https://doi.org/10.1128/mSystems.00029-16.
32. Lieberman TD, Michel J-B, Aingaran M, Potter-Bynoe G, Roux D, Davis MR, Skurnik D, Leiby N, LiPuma JJ, Goldberg JB, McAdam AJ, Priebe GP, Kishony R. 2011. Parallel bacterial evolution within multiple patients identifies candidate pathogenicity genes. Nat Genet 43:1275–1280. https://doi.org/10.1038/ng.997.
33. Ferreira AS, Leitão JH, Sousa SA, Cosme AM, Sá-Correia I, Moreira LM. 2007. Functional analysis of *Burkholderia cepacia* genes *bceD* and *bceF*, encoding a phosphotyrosine phosphatase and a tyrosine autokinase, respectively: role in exopolysaccharide biosynthesis and biofilm formation. Appl Environ Microbiol 73:524–534. https://doi.org/10.1128/AEM.01450-06.
34. Sambrook J, Russell DW. 2001. Molecular cloning: a laboratory manual, 3rd ed. Cold Spring Harbor Laboratory Press, Cold Spring Harbor, NY.
35. Pfaffl MW. 2001. A new mathematical model for relative quantification in real-time RT-PCR. Nucleic Acids Res 29:e45. https://doi.org/10.1093/nar/29.9.e45.
36. Li C, Wong WH. 2001. Model-based analysis of oligonucleotide arrays: model validation, design issues and standard error application. Genome Biol 2:RESEARCH0032. https://doi.org/10.1186/gb-2001-2-8-research0032.
37. Li C, Wong WH. 2001. Model-based analysis of oligonucleotide arrays: expression index computation and outlier detection. Proc Natl Acad Sci U S A 98:31–36. https://doi.org/10.1073/pnas.98.1.31.
38. Caiazza NC, O'Toole GA. 2004. SadB is required for the transition from reversible to irreversible attachment during biofilm formation by *Pseudomonas aeruginosa* PA14. J Bacteriol 186:4476–4485. https://doi.org/10.1128/JB.186.14.4476-4485.2004.
39. Altschul SF, Madden TL, Schaffer AA, Zhang J, Zhang Z, Miller W, Lipman DJ. 1997. Gapped BLAST and PSI-BLAST: a new generation of protein database search programs. Nucleic Acids Res 25:3389–3402. https://doi.org/10.1093/nar/25.17.3389.
40. Winsor GL, Khaira B, Van Rossum T, Lo R, Whiteside MD, Brinkman FS. 2008. The Burkholderia Genome Database: facilitating flexible queries and comparative analyses. Bioinformatics 24:2803–2804. https://doi.org/10.1093/bioinformatics/btn524.
41. Thompson JD, Higgins DG, Gibson TJ. 1994. CLUSTAL W: improving the sensitivity of progressive multiple sequence alignment through sequence weighting, position-specific gap penalties and weight matrix choice. Nucleic Acids Res 22:4673–4680. https://doi.org/10.1093/nar/22.22.4673.
42. Tamura K, Stecher G, Peterson D, Filipski A, Kumar S. 2013. MEGA6: Molecular Evolutionary Genetics Analysis version 6.0. Mol Biol Evol 30:2725–2729. https://doi.org/10.1093/molbev/mst197.
43. Vandamme P, Holmes B, Vancanneyt M, Coenye T, Hoste B, Coopman R, Revets H, Lauwers S, Gillis M, Kersters K, Govan JR. 1997. Occurrence of multiple genomovars of *Burkholderia cepacia* in cystic fibrosis patients and proposal of *Burkholderia multivorans* sp. nov. Int J Syst Bacteriol 47:1188–1200. https://doi.org/10.1099/00207713-47-4-1188.
44. Mahenthiralingam E, Coenye T, Chung JW, Speert DP, Govan JR, Taylor P, Vandamme P. 2000. Diagnostically and experimentally useful panel of strains from the *Burkholderia cepacia* complex. J Clin Microbiol 38:910–913.
45. Ferreira AS, Silva IN, Fernandes F, Pilkington R, Callaghan M, McClean S, Moreira LM. 2015. The tyrosine kinase BceF and the phosphotyrosine phosphatase BceD of *Burkholderia contaminans* are required for efficient invasion and epithelial disruption of a cystic fibrosis lung epithelial cell line. Infect Immun 83:812–821. https://doi.org/10.1128/IAI.02713-14.
46. Coenye T, Vandamme P, LiPuma JJ, Govan JR, Mahenthiralingam E. 2003. Updated version of the *Burkholderia cepacia* complex experimental strain panel. J Clin Microbiol 41:2797–2798. https://doi.org/10.1128/JCM.41.6.2797-2798.2003.
47. Larsen GY, Stull TL, Burns JL. 1993. Marked phenotypic variability in *Pseudomonas cepacia* isolated from a patient with cystic fibrosis. J Clin Microbiol 31:788–792.
48. Nelson MJ, Montgomery SO, O'Neill EJ, Pritchard PH. 1986. Aerobic metabolism of trichloroethylene by a bacterial isolate. Appl Environ Microbiol 52:383–384.
49. LiPuma JJ, Mortensen JE, Dasen SE, Edlind TD, Schidlow DV, Burns JL, Stull TL. 1988. Ribotype analysis of *Pseudomonas cepacia* from cystic fibrosis treatment centers. J Pediatr 113:859–862. https://doi.org/10.1016/S0022-3476(88)80018-0.
50. Figurski DH, Helinski DR. 1979. Replication of an origin-containing derivative of plasmid RK2 dependent on a plasmid function provided in *trans*. Proc Natl Acad Sci U S A 76:1648–1652. https://doi.org/10.1073/pnas.76.4.1648.
51. Sokol PA, Darling P, Woods DE, Mahenthiralingam E, Kooi C. 1999. Role of ornibactin biosynthesis in the virulence of *Burkholderia cepacia*: characterization of *pvdA*, the gene encoding L-ornithine N(5)-oxygenase. Infect Immun 67:4443–4455.
52. Vieira J, Messing J. 1991. New pUC-derived cloning vectors with different selectable markers and DNA replication origins. Gene 100:189–194. https://doi.org/10.1016/0378-1119(91)90365-I.
53. Kovach ME, Phillips RW, Elzer PH, Roop RM, II, Peterson KM. 1994. pBBR1MCS: a broad-host-range cloning vector. Biotechniques 16:800–802.